2022-12

SUB-SEASONAL FORECASTS OF ATMOSPHERIC RIVERS IMPACTING CALIFORNIA AND SOUTHERN EUROPE UTILIZING STREAMFUNCTION ANOMALIES

Rueter, Niklas H.

Monterey, CA; Naval Postgraduate School

NAVAL POSTGRADUATE SCHOOL

MONTEREY, CALIFORNIA

THESIS

SUB-SEASONAL FORECASTS OF ATMOSPHERIC RIVERS IMPACTING CALIFORNIA AND SOUTHERN EUROPE UTILIZING STREAMFUNCTION ANOMALIES

by

Niklas H. Rueter

December 2022

Thesis Advisor: Wendell A. Nuss
Second Reader: Mark A. Boothe

THIS PAGE INTENTIONALLY LEFT BLANK

REPORT DOCUMENTATION PAGE	*Form Approved OMB No. 0704-0188*

Public reporting burden for this collection of information is estimated to average 1 hour per response, including the time for reviewing instruction, searching existing data sources, gathering and maintaining the data needed, and completing and reviewing the collection of information. Send comments regarding this burden estimate or any other aspect of this collection of information, including suggestions for reducing this burden, to Washington headquarters Services, Directorate for Information Operations and Reports, 1215 Jefferson Davis Highway, Suite 1204, Arlington, VA 22202-4302, and to the Office of Management and Budget, Paperwork Reduction Project (0704-0188) Washington, DC, 20503.

1. AGENCY USE ONLY *(Leave blank)*	**2. REPORT DATE** December 2022	**3. REPORT TYPE AND DATES COVERED** Master's thesis

4. TITLE AND SUBTITLE
SUB-SEASONAL FORECASTS OF ATMOSPHERIC RIVERS IMPACTING CALIFORNIA AND SOUTHERN EUROPE UTILIZING STREAMFUNCTION ANOMALIES

5. FUNDING NUMBERS

6. AUTHOR(S) Niklas H. Rueter

7. PERFORMING ORGANIZATION NAME(S) AND ADDRESS(ES) Naval Postgraduate School Monterey, CA 93943-5000	**8. PERFORMING ORGANIZATION REPORT NUMBER**
9. SPONSORING / MONITORING AGENCY NAME(S) AND ADDRESS(ES) N/A	**10. SPONSORING / MONITORING AGENCY REPORT NUMBER**

11. SUPPLEMENTARY NOTES The views expressed in this thesis are those of the author and do not reflect the official policy or position of the Department of Defense or the U.S. Government.

12a. DISTRIBUTION / AVAILABILITY STATEMENT Approved for public release. Distribution is unlimited.	**12b. DISTRIBUTION CODE** A

13. ABSTRACT (maximum 200 words)

Atmospheric rivers (ARs) are narrow plumes of moisture that transport a large flux of water vapor into the mid-latitudes. This source of precipitation is vital for the U.S. West Coast, especially California, where seasonal precipitation is highly dependent on these ARs and accounts for up to half its annual precipitation. Due to the reliance on ARs for precipitation, effective water management has become crucial in the U.S. West as wildfires worsen and populations grow, increasing the demand on the entire region's reservoirs. It is imperative that AR events are forecasted and communicated as early as possible. That is the goal of this thesis, to extend the prediction of ARs into the sub-seasonal timescale. Analysis of streamfunction anomalies (SFA) and the vertical integral of the divergence of geopotential flux (DGF) were done via an anomaly box off the west coast of British Columbia, with the process replicated for a climatologically similar region in the North Atlantic, showing good success to at least 40 days prior to an AR event for both San Francisco and Lisbon, Portugal. This lead time of conditions supporting ARs impacting these two regions is invaluable for forecasters and affiliated stakeholders. While this method will not forecast specific AR events, it can statistically indicate whether more ARs will be likely at the sub-seasonal time scale. The past 28 years of data (1994–2021) were analyzed for trends in SFA and DGF across both anomaly boxes.

14. SUBJECT TERMS atmospheric rivers, ARs, streamfunction, California, U.S. West Coast, geopotential height, anomalies, sub-seasonal, forecasts, Southern Europe, Lisbon, San Francisco, Iberian Peninsula, vertical integral of divergence of geopotential flux	**15. NUMBER OF PAGES** 81
	16. PRICE CODE

17. SECURITY CLASSIFICATION OF REPORT	**18. SECURITY CLASSIFICATION OF THIS PAGE**	**19. SECURITY CLASSIFICATION OF ABSTRACT**	**20. LIMITATION OF ABSTRACT**
Unclassified	Unclassified	Unclassified	UU

NSN 7540-01-280-5500

Standard Form 298 (Rev. 2-89)
Prescribed by ANSI Std. 239-18

THIS PAGE INTENTIONALLY LEFT BLANK

Approved for public release. Distribution is unlimited.

SUB-SEASONAL FORECASTS OF ATMOSPHERIC RIVERS IMPACTING CALIFORNIA AND SOUTHERN EUROPE UTILIZING STREAMFUNCTION ANOMALIES

Niklas H. Rueter
Lieutenant Commander, United States Navy
BS, Purdue University, 2012

Submitted in partial fulfillment of the
requirements for the degree of

MASTER OF SCIENCE IN METEOROLOGY AND PHYSICAL OCEANOGRAPHY

from the

NAVAL POSTGRADUATE SCHOOL
December 2022

Approved by: Wendell A. Nuss
Advisor

Mark A. Boothe
Second Reader

Wendell A. Nuss
Chair, Department of Meteorology

THIS PAGE INTENTIONALLY LEFT BLANK

ABSTRACT

Atmospheric rivers (ARs) are narrow plumes of moisture that transport a large flux of water vapor into the mid-latitudes. This source of precipitation is vital for the U.S. West Coast, especially California, where seasonal precipitation is highly dependent on these ARs and accounts for up to half its annual precipitation. Due to the reliance on ARs for precipitation, effective water management has become crucial in the U.S. West as wildfires worsen and populations grow, increasing the demand on the entire region's reservoirs. It is imperative that AR events are forecasted and communicated as early as possible. That is the goal of this thesis, to extend the prediction of ARs into the sub-seasonal timescale. Analysis of streamfunction anomalies (SFA) and the vertical integral of the divergence of geopotential flux (DGF) were done via an anomaly box off the west coast of British Columbia, with the process replicated for a climatologically similar region in the North Atlantic, showing good success to at least 40 days prior to an AR event for both San Francisco and Lisbon, Portugal. This lead time of conditions supporting ARs impacting these two regions is invaluable for forecasters and affiliated stakeholders. While this method will not forecast specific AR events, it can statistically indicate whether more ARs will be likely at the sub-seasonal time scale. The past 28 years of data (1994–2021) were analyzed for trends in SFA and DGF across both anomaly boxes.

THIS PAGE INTENTIONALLY LEFT BLANK

TABLE OF CONTENTS

THIS PAGE INTENTIONALLY LEFT BLANK

LIST OF FIGURES

LIST OF TABLES

THIS PAGE INTENTIONALLY LEFT BLANK

LIST OF ACRONYMS AND ABBREVIATIONS

AMS	American Meteorological Society
AR	Atmospheric River
BC	British Columbia
C3S	Copernicus Climate Change Service
CA	California
CFSR	Climate Forecast System Reanalysis
CPC	Climate Prediction Center
CSI	Critical Success Index
CWW	California Water Watch
DGF	(Vertical Integral of) Divergence of Geopotential Flux
ECMWF	European Centre for Medium-Range Weather Forecasts
ENSO	El Nino-Southern Oscillation
ERA5	Earth Reanalysis 5
FAR	false alarm ratio
FIRO	Forecast Informed Reservoir Operations
GFS	Global Forecast System
GIUK	Greenland-Iceland-United Kingdom
HSS	Heidke skill score
IVT	integrated vertical transport
KDE	kernel density estimation
MJO	Madden Julian Oscillation
NOAA	National Oceanic and Atmospheric Administration

NWS	National Weather Service
POD	probability of detection
PSL	Physical Sciences Laboratory
QBO	Quasi-Biennial Oscillation
SF	San Francisco
SFA	Streamfunction Anomaly
SR	Success ratio
TPW	total precipitable water

ACKNOWLEDGMENTS

First and foremost, I'd like to thank my advisor, Dr. Wendell Nuss. His guidance and mentorship throughout this process was invaluable in ensuring this thesis was a success and something that I could be proud of. His incredible expertise in the field combined with his hands-off approach really allowed me to take ownership of this study and learn a tremendous amount during my time with him. His presence during the turbulent years of COVID made a huge impact for not just my experience at NPS, but for many previous students whom he impacted.

To my cohort, NPS faculty, and my second reader, Mark Boothe. All of them were instrumental in getting through the first 18 months of this 30-month program conducted via distance learning thanks to COVID. It was a frustrating and challenging experience, but everyone supported each other to make the most of it, and it made being back in person that much sweeter.

Last but certainly not least, thank you to my wife and family for their support throughout this process. I will cherish the time we had together while at NPS, and I deeply appreciate the love and encouragement needed to complete this thesis.

THIS PAGE INTENTIONALLY LEFT BLANK

I. INTRODUCTION

A. MOTIVATION

The first time I heard the term "atmospheric river" was while I was attending the Naval Postgraduate School (NPS) in Monterey, California (CA) in late January of 2021. I was surprised to find out that these weather events can produce up to 70% of the annual precipitation totals for much of U.S. West Coast, but especially so for CA. With the extremely active and deadly fire seasons of 2016, 2018, and 2020 across much of CA in conjunction with sustained below average rainfall from 2018–2022, it became apparent to me that Atmospheric Rivers (ARs) were essential sources of seasonal precipitation, with that importance only growing over the coming decades as climate change exacerbates the desertification of much of CA. Due to its climate that relies on seasonal precipitation, that is rainfall confined to less than 6 months out of the year, a complex and robust reservoir system and management is essential for the state to get through each year. This being understood, I believe there is immense demand and opportunity for improvement in the forecasting lead time of ARs. The standard 10-day lead time is insufficient when you consider all the end users affected by the decision makers who control these water systems. Sub-seasonal forecasting can provide lead times of 30, 60, and even 90 days, which would tremendously improve water managers' ability to allocate resources depending on the forecast regarding ARs.

Just over the past few years, 2020–2022, during which CA has been in a La Niña pattern and a period of below average rainfall, the reservoir storage not only in CA, but throughout the West Coast, and Southwest U.S, has dramatically declined. This has gained national attention with most of the region grappling with severe water restrictions. Reservoirs across the West, such as Lake Mendocino, Lake Oroville, Lake Shasta, and Lake Mead in Nevada have been at historically low levels, with water levels dropping to those never seen since their creation. Figure 1 shows Lake Shasta in Northern CA and Lake Mead in Arizona as seen in 2021. These two reservoirs are among the biggest in the U.S. and provide a large portion of water for the U.S. West. In 2021 when these images were taken, Lake Shasta was at its lowest water level since 1945, and Lake Mead was at

its lowest since the 1930s. Ironically, these dates are when these reservoirs were first constructed and filled.

Figure 1. Lake Shasta (left) and Lake Mead (right). Both images are from 2021 when the reservoirs were at record low levels. Source: Public Policy Institute of California and Smithsonian Magazine (2021).

This attention on reservoir levels has brought recent attention to the importance of ARs on the region's water supply and storage. Cooperative efforts have begun between meteorologists and water managers such as the Forecast Informed Reservoir Operations (FIRO) that "uses data from watershed monitoring and improved weather and hydrologic forecasting to help water managers selectively retain or release water from reservoirs…and that leverages advancements in the science of meteorological and hydrological forecasting" (FIRO, 2022).

As of the fall of 2022, the California Water Watch (CWW), a department of its parent organization, the California Data Exchange Center, and California Department of Water Resources, has completed a comprehensive analysis of the dire situation regarding California's water situation. "Weather extremes brought on by climate change have reduced our water supply. We are in a third year of drought and need to use less water. January, February, and March (of 2022) had the least rain and snow in over 100 years, with just six inches of precipitation observed across the Sierra Nevada. These warm, dry months overshadowed gains in precipitation at the end of 2021. Snow melted faster than

expected, reducing snowpack to just 38% of average by April 1st. A growing body of evidence is starting to show that our current drought is an extension of the 2012–2016 drought, interrupted by just a few wet years" (CWW, 2022). This strain on CA, and the Southwest U.S., will continue to create a strain on all aspects of the hydrologic management community, highlighting the motivation for this study to better understand and forecast ARs at a longer lead time. Figure 2 highlights that as of 30 August 2022, nearly every major reservoir in the California Department of Water Resources is significantly below the percentage of historical average, with the majority of the reservoir water levels below 33% of total capacity. This is a testament to multiple years of sustained drought and below average AR activity.

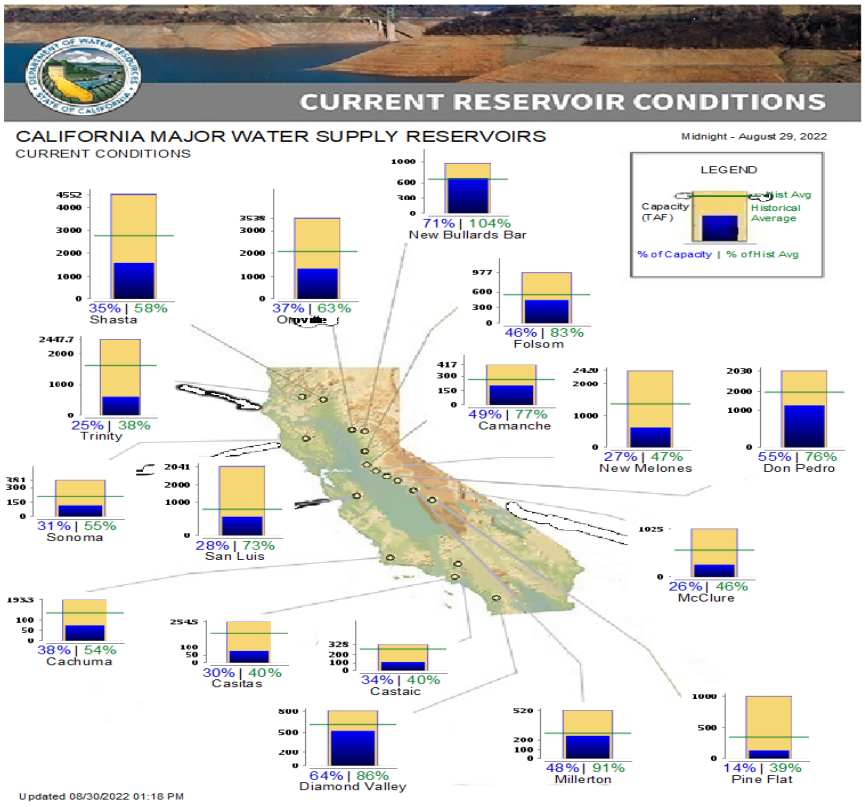

Figure 2. CA reservoir water levels in thousands of acre-feet (TAF). Accessed on 30 Aug 2022. Source: California Department of Water Resources at cdec.water.ca.gov (2022).

The attention ARs have received has outpaced the meteorological and water management communities, as Congress has now targeted AR forecasts as a tool to manage climate change, "With climate change bringing more extreme rain events, the U.S. federal government is taking greater notice of ARs. In December 2021 the National Oceanographic and Atmospheric Administration's (NOAA) Science Advisory Board sent a formal set of recommendations for the next decade, "Priorities for Weather Research," to policy makers in Congress. The recommendations call out the need for better information on ARs to support reservoir operation, among other things" (Ralph, 2022).

It is clear there is a significant problem with water management in the U.S. West; therefore, this study was motivated to use meteorological dynamics and forecasting to bridge the gap between the meteorological and water management sectors. The hope of this study is that the tools identified will aid forecasters, water sector managers, governmental agencies, and many more to aid in the solving of this growing problem.

B. MILITARY APPLICATION

The United States Navy conducts operations globally, but two significant areas and the focus of this study are the regions of the U.S. West Coast and the West Coast of Europe. While Rota, Spain is the only port on the West Coast of Europe where U.S. ships are homeported, U.S. ships make frequent port visits with allies up and down the West Coast. Additionally, the Straits of Gibraltar are one of the most crucial transit lanes in the world, so the impact of adverse weather conditions on the safe passage of ships, along with the complexity of flight operations can be significantly hampered by weather systems such as ARs. Forecasts with a lead time of 20 days or more of adverse events like ARs during the winter months would be invaluable for transiting U.S. Navy ships and flight operations throughout the Western Europe Sea lanes and U.S. West Coast operating areas. This would be an additional tool that forecasters at Fleet Weather Centers (FWC) could use to improve ship routing forecasting, increasing military readiness through increased operations, and more importantly increased safety of ships at sea. This method could translate to other areas the U.S. Navy operates that are affected by

ARs, to include the East China Sea and Japan, Northwest Africa, the West Coast of South America, and the Coral Sea.

C. GOALS OF STUDY

This study aims to provide forecast lead time of 20 days to as much as 40 days for AR events in multiple geographic locations. There is a significant gap between medium-range forecasting, which is the standard model limitation of 10–16 days, and seasonal forecasts such as those produced by the National Weather Service (NWS) Climate Prediction Center (CPC). These CPC seasonal outlooks are produced for generally 90-day outlooks. This gap, known as the sub-seasonal timescale, is the focus of this study. There is significant opportunity in improving the sub-seasonal timescale, which is approximately 2–5 weeks. This study aims to utilize streamfunction anomaly (SFA) at the 250mb level, which can provide greater than 20 days early indication of favorable conditions that synoptically support ARs. While this method does not have the granularity to forecast specific AR events, it can statistically indicate whether ARs will be more likely or not at the sub-seasonal timescale. The study was extended to a similar setup off the West Coast of Europe, where similar synoptic conditions setup for ARs, which are of similar importance to the water budget of the Iberian Peninsula and Western France. The ability to have even a 60–70% confidence that an AR will occur in a geographic area at 20, 30, or 40 days is beyond the current model prediction capability; the Global Forecast System (GFS) model for example, only runs out to 16 days. The ability to extend this forecast range for ARs with skill would have significant benefits across a multitude of sectors of society.

THIS PAGE INTENTIONALLY LEFT BLANK

II. BACKGROUND

Over the last decade, the term Atmospheric River has exploded in use and is now broadly used by forecasters and the public sector alike to identify any significant rainfall event impacting the U.S. West Coast, and specifically CA. While an argument can certainly be made about the overuse of this label, the value of identifying ARs as a vital component of the meteorological cycle for the CA and U.S. West Coast's climatology cannot be overstated. Officially, an AR is defined by the American Meteorological Society (AMS) as, "A long, narrow, and transient corridor of strong horizontal water vapor transport that is typically associated with a low-level jet stream ahead of the cold front of an extratropical cyclone. The water vapor in atmospheric rivers is supplied by tropical and/or extratropical moisture sources" (AMS, 2022). Figure 3 shows an illustration of the generic structure of an AR.

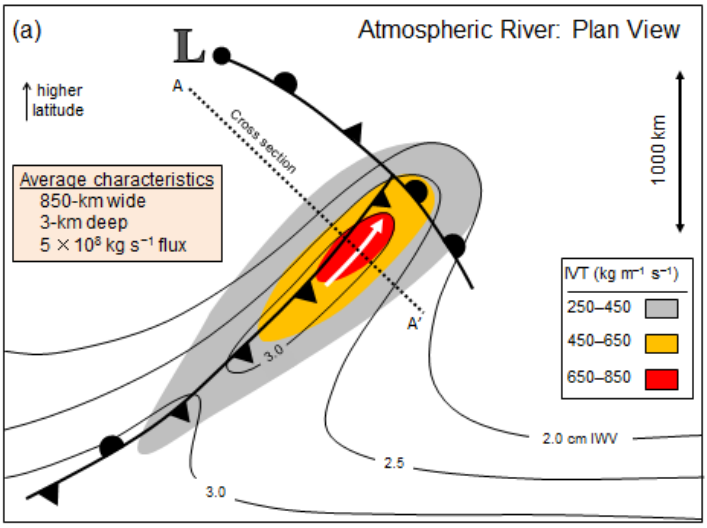

Figure 3. Plan view of the structure of an AR. Key feature is the midlatitude forcing along the cold front axis, represented by the IVT shading. This combines with the high moisture provided from the southerly flow of water vapor. Source: AMS Glossary of Meteorology (2022).

The short-term synoptic setup for ARs is understood well, consisting of a midlatitude cyclone tapping into a water vapor reservoir that is broad in nature,

sometimes extending for hundreds to thousands of miles to the south/southwest towards the tropics. However, beyond the typical forecast confidence of 5–7 days, less is understood about longer-range indicators of AR events (Guirguis et al. 2018). Previous work on ARs has continued to build on their understanding, aided by the increased focus and understanding of their significance (Ralph et al. 2017), with work by Justin Van Es suggesting a dipole interaction of high and low pressures being critical to form major ARs (Van Es, 2020). While high and low pressures are inherently dynamic and therefore transient in nature, anomalous pressure patterns such as an omega-block or rex-block can persist for timescales of weeks. Consequently, the geopotential height or streamfunction anomalies will highlight these types of persistent patterns.

A. PRIOR RESEARCH

A comprehensive paper, titled, "Climatology and Variability of Atmospheric Rivers over the North Pacific" (Mundhenk, 2017), found a strong relationship between geopotential height anomaly patterns and the occurrence of ARs. This study provided the background information on the climatology of ARs impacting the Central Coast of CA and confirmed the broad scope and impact of ARs. He points out "At times considered to be only rare or extreme events, analyses emphasize that ARs are nearly ever-present contributors to the hydrological cycle on a basin-wide scale" (Mundhenk, 2017). His analysis shows that a region of 'geopotential height anomaly' resulted after taking the difference between the geopotential heights at 500mb over 400 AR event composites from December, January, and February (DJF) for Gulf of Alaska and U.S. West Coast AR landfalls.

Figure 4 shows the composite of 461 U.S. West Coast ARs (left panel) and the composite of 383 Gulf of Alaska ARs (right panel), with both being DJF months only. The two panels show the average geopotential height for their respective AR setups. To create Figure 5, Mundhenk took the difference between these two panels. This results in a positive difference because essentially a trough on the left-hand side image is being subtracted from a ridge in the same location in the right-hand side image of Figure 4. This height anomaly box, as shown in Figure 5, was identified as the region of maximum

geopotential height variability that influences ARs for either Alaska or the U.S. West Coast. An important distinction when looking at Figure 5 is that the red shading does not represent the strength of the anomaly for either the Gulf of Alaska AR scenario or the U.S. West Coast scenario, but rather the magnitude of the difference between the two scenarios. The red shading is representative of a positive geopotential height difference. This is an extremely important observation, as the anomaly box captures the region of highest variability and therefore further analysis of this anomaly box, outlined in green in Figure 5, and its implications regarding ARs are the focus of this study.

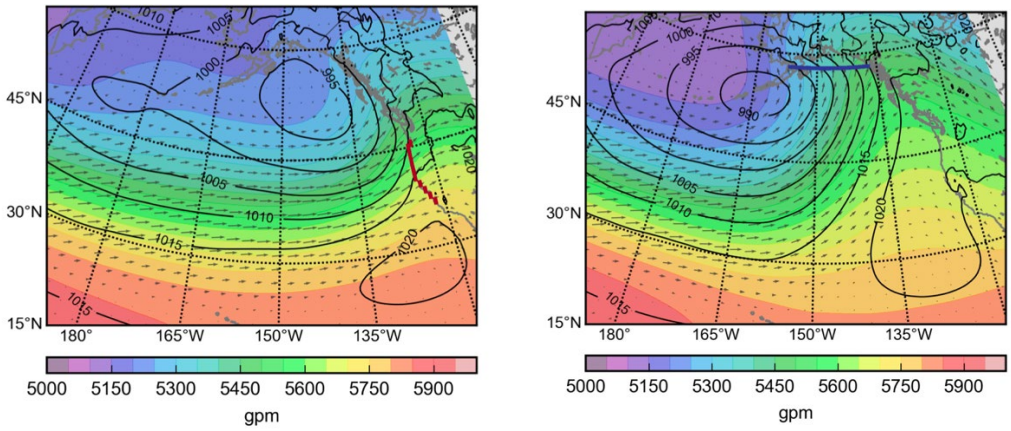

Figure 4. U.S. West Coast AR event composite (left), Gulf of Alaska AR event composite (right) during DJF of 37 years (1979–2015). Shading is 500mb geopotential height overlaid with sea level pressure contoured with black lines and 700mb vector winds (arrows). Note the area impacted by an AR event denoted by a red line along the U.S. West Coast (left) and a blue line across the Gulf of Alaska (right). Source: Mundhenk (2017).

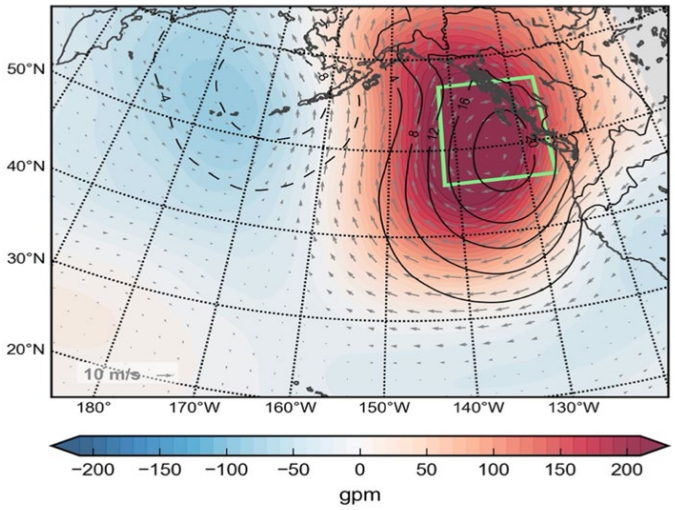

Figure 5. 500 mb geopotential height anomaly difference between Alaska and U.S. West Coast AR composites during DJF of 37 years (1979–2015). Shading is 500mb geopotential height difference overlaid with sea level pressure contoured with black lines (4mb intervals), and 700mb vector winds (arrows). The outlined box shows the region of highest variability of dynamics for AR events. Source: Mundhenk (2017).

Figure 6 shows that a negative geopotential height anomaly value in the region of variability is associated with U.S. West Coast ARs, while a positive geopotential height anomaly value in the same region is associated with Gulf of Alaska ARs. This analysis was done using monthly averages.

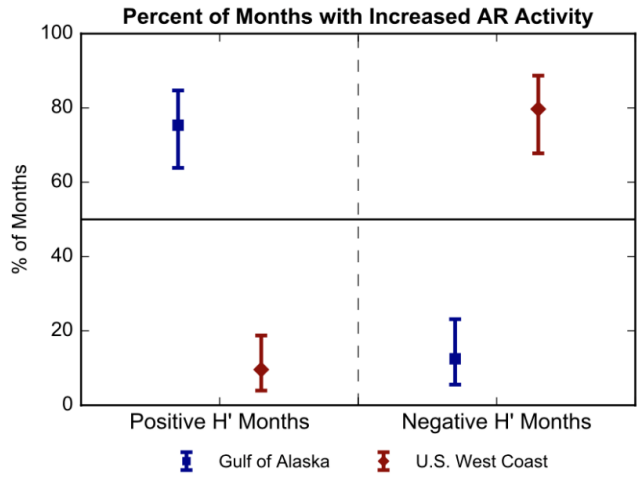

Figure 6. Plot showing the correlation between negative geopotential height and AR activity for the U.S. West Coast. The reverse is the case for the Gulf of Alaska. H` represents height anomalies from the outlined box in Figure 5. Source: Mundhenk (2017).

This link provides a crucial relationship to the sub-seasonal timeframe, and over the 37-year period Mundhenk conducted this study, it shows that this height anomaly box represents the majority of AR events, not just a few outlier events. This strong signal was observed to occur for the monthly averages of when an AR occurred, but if the signal is present in preceding months, then longer-term prediction may be feasible. This idea, in combination with the fact that the work of Mundhenk showed that the concept of using a height anomaly box could work for the U.S., but went no further, provided the direction to build on Mundhenk's work. By applying the process of a height anomaly box shown to work for the U.S., this study aimed to provide more robust results by applying it to a new region, Southern Europe. Additionally, the analysis done in Figures 4–6 was done over 461 AR events at the time of the event, and the monthly averages during those months. It is the belief of this author that a significant growth opportunity existed in taking this process and using it as a forecast tool, to step back weeks and months prior to the AR event and analyze if the patterns identified in this prior research continued.

This study focused near exclusively on the October-March months, which was based on climatology of ARs. This seasonality of ARs impacting the U.S. West Coast is

illustrated in Figure 7 and combines the previously mentioned correlation of the geopotential height anomaly.

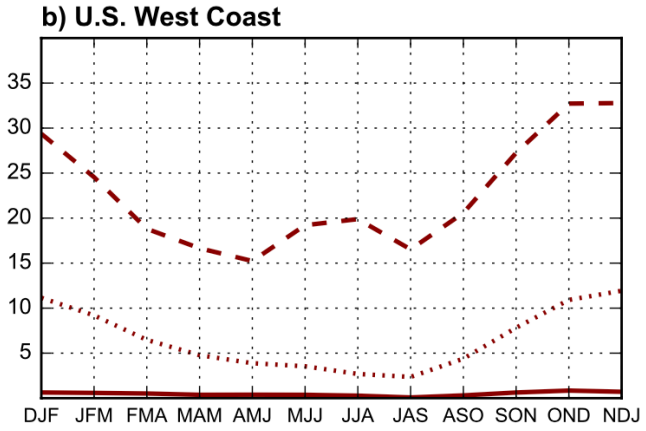

Figure 7. Seasonality of ARs impacting the U.S. West Coast. Dashed line is under a negative geopotential height anomaly regime, solid line is a positive geopotential height anomaly, and dotted line is the mean seasonality. Vertical axis is AR frequency (%) calculated over the 37-year period (1979-2015). Source: Mundhenk (2017).

AR frequency peaks in the November-December-January 90-day period and is near zero in the June-July-August 90-day period. This seasonality limitation of ARs impacting the U.S. West Coast and similar latitudes allowed the data analysis for this study to be limited exclusively to the October-March months.

B. STREAMFUNCTION

Streamfunction is more comprehensive when looking at dynamics than a standard geopotential height because it highlights flow in tropical and sub-tropical regions where geopotential heights are relatively uniform. Streamfunction is defined as;

$$u=-\partial\Psi/\partial y;\ v=\partial\Psi/\partial x$$

where Ψ is the streamfunction and captures the non-divergent part of a horizontal flow. In higher latitudes where the flow is closer to geostrophic, the streamfunction and geopotential height are essentially the same except for a factor of g/f ($\Psi=gz/f$). Thus, in

the midlatitudes the geopotential height and streamfunction show similar features. For lower latitudes, the Coriolis parameter is minimal; therefore, streamfunction can identify circulations more easily even though the geopotential height variations are quite small.

Streamfunction is in sigma vertical coordinates for the dataset used in this study, so the level of .2582 was used as it is approximately equivalent to 250mb. In principle, cyclonically curved streamfunction in the upper levels are indicative of an upper-level trough, which is conducive to surface low pressure and rainfall. This is similar to geopotential height, which is the standard for identifying and analyzing pressure changes and synoptic development. Geopotential height anomalies are commonly used as well to determine patterns and deviations from normal that may be more strongly forced than usual. The reason for this is that the anomaly is calculated by subtracting the climatological mean from the observed value for the period in question. Therefore, this 'departure from the mean' is what stands out and warrants further investigation. The same approach can be applied to the streamfunction to create streamfunction anomalies (SFA) to highlight regions of enhanced or diminished circulation in a particular region, including the lower latitudes.

C. RESEARCH QUESTIONS

The prior research summarized in the previous section alluded to a height anomaly box that was utilized to indicate AR activity across synoptic and sub-seasonal timescales. The goal of this study is therefore to extrapolate that process and apply it using SFA, due to the limitations of geopotential height at low latitudes as outlined in the previous section. This valuable utility of a specific area motivated this study to answer the following research questions:

1. Using SFA in place of geopotential height anomaly, can these anomalous regions be used to bridge the gap of forecasting between medium-range forecasts (up to 16 days) and seasonal forecasts (3+ months), thereby increasing forecast skill of ARs and providing increased lead time at the sub-seasonal timescale?

2. Can this process of identifying an anomaly region be applied to other regions around the world?

3. Does the strength of the anomaly translate to strength of the subsequent AR events?

III. DATA AND METHODS

A. DATA

1. Focus Regions

For this study, the initial focus region was off the British Columbia (BC) West Coast as described in the prior research of Mundhenk. This region was chosen as the area with the highest dynamic variability and therefore likely the greatest importance to the setup of conditions which support ARs on the CA Coast. To pair this region of SFA analysis with a coastal site, San Francisco (SF) was chosen as it is located on the Central Coast of CA, has historical records at the NWS site at the SF airport, and most importantly, unlike nearby locations to the north and south, is not influenced by coastal topography that greatly affects rainfall amounts via upslope enhancement. The region of focus is shown in Figure 8 and has latitude bounds of 57°N and 45°N, with longitude bounds of 142°W and 127°W.

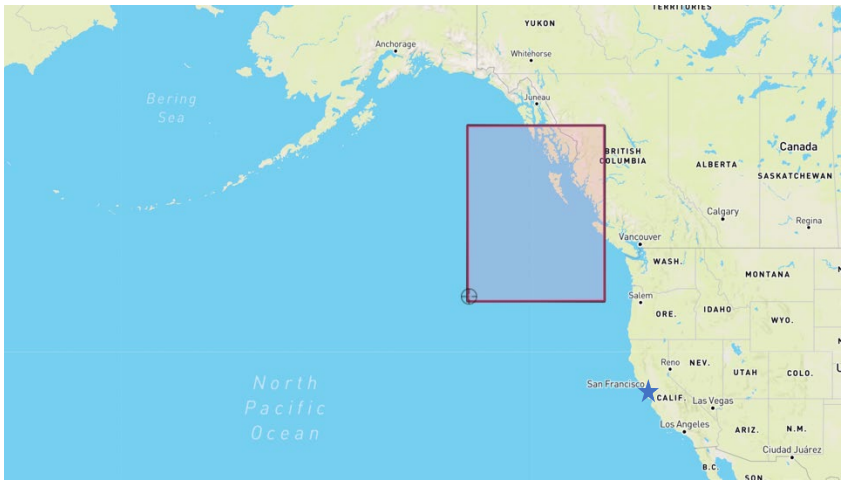

Figure 8. BC West Coast analysis box with blue star indicating San Francisco. Adapted from Bounding Box Tool, bbboxfinder.com.

A timespan of 28 years, 1994–2021, was used to capture multiple cycles of the El Nino-Southern Oscillation (ENSO), which does have an impact on the amount of precipitation the climatological pattern supports for the CA coast. It also includes

significant AR events over the period, as well as significant dry winters where no ARs occurred for contrast.

To extend the potential application of streamfunction anomaly to predicting ARs more generally, the process was shifted to a new geographic region. The goal was to mirror the climatology of the CA Central Coast and Western Europe, specifically the Iberian Peninsula, where rainfall that is similarly limited to the winter months fits that criteria (Zavadoff and Kirtman 2020; Doiteau et al. 2021). Water management is just as critical in the Iberian Peninsula as it is in the American West, as a few years of sustained drought can lead to extreme water shortages such as those experienced by CA. Initially, Santiago de Compostela was chosen in the northwest corner of Spain. However, its number of months where an AR event occurred vastly exceeded the number for SF. Also, Santiago de Compostela is located at 42.8°N, which is over 5° of latitude north of SF. This 5° shift northward clearly has a significant impact on AR activity, as you would see if you shifted 5° north on the CA coast. A more climatologically similar location to SF was desired, so Lisbon, Portugal was chosen. Lisbon lies at 38.7°N which is almost identical to the 37.6°N latitude of SF.

Figure 9. Google Maps image indicating the two locations chosen for this study. Source: Google Maps (2022).

The region we identified as having the highest variability in geopotential height, and therefore, SFA, that could be an indicator for cyclonic development supporting ARs

in the North Atlantic Ocean was west of Ireland and south of Iceland, close to the commonly known "GIUK gap," which is short for Greenland-Iceland-United Kingdom. This region was identified based on where the climatological upper-level low pressure is positioned in the North Atlantic, shown in Figure 11 with the geopotential height anomaly at 250mb during the climatological winter (October-March) over the period of this study, 1994–2021. The position of the analysis box was chosen to capture where the SFA (synonymous with geopotential height in Figure 11) signal is most indicative of an AR that would affect Lisbon. For consistency, the size of the analyzed region matched the size of the one used off the U.S. West Coast, which was 15° in longitudinal width and 12° in latitudinal width. The bounds of the European box, 57°N to 45°N and 28°W to 13°W, were matched in latitude to those of the BC West Coast box and is shown in Figure 10.

Figure 10. European analysis box with blue star indicating Lisbon, Portugal. Adapted from Bounding Box Tool, bbboxfinder.com

To show the relationship that these two regions may have to each other, Figure 11 shows the entire Pacific and Atlantic Ocean basins with the analysis boxes overlaid. In the winter months over the 28-year period, the two analysis boxes capture the most negative geopotential heights, which confirmed the proper placement of their location for SFA analysis. Additionally, they may occur in similar parts of the wave suggesting that

their activity may be coupled. The two forcing regions are centered roughly 15° to the north and west of the analysis cities to best capture the SFA forcing for an AR. A previous study showed that there is typically a dipole interaction between (1) high pressure anticyclonic winds on the southeastern flank of the AR that feed tropical moisture into the AR and (2) cyclonic winds off the low-pressure system to the northwest, resulting in convergent flow along the AR (Van Es, 2020). While that is the expected synoptic setup for an AR, this study focused on the negative SFA associated with the trough, and the climatological pattern of both geopotential height and SFA support that these boxes capture the peak of the negative SFA and therefore the peak forcing for ARs affecting SF and Lisbon.

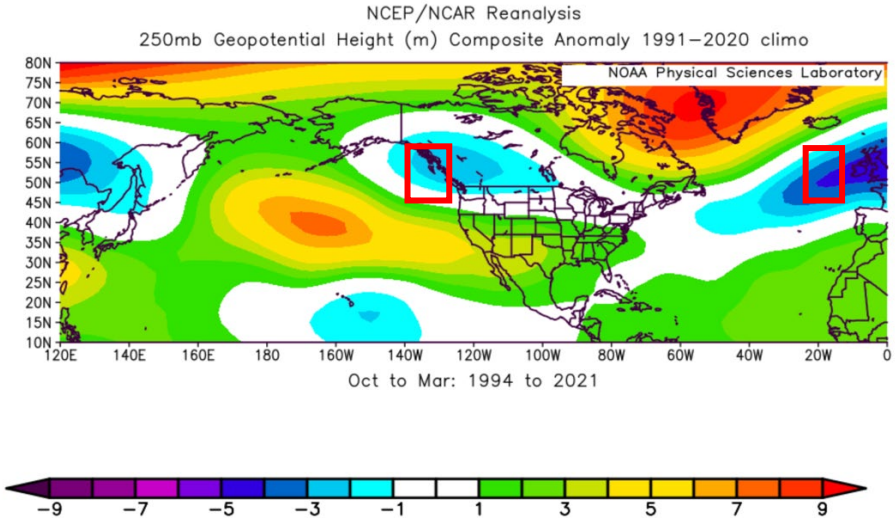

Figure 11. 250mb geopotential height anomaly average across all 168 AR months (ONDJFM) of the 28-year period (1994–2021) of this study, with analysis boxes overlaid in red. This anomaly is calculated against the entire 1991–2020 climate reanalysis dataset. Source: NOAA/ESRL Physical Sciences Laboratory, Boulder Colorado from their website at http://psl.noaa.gov/.

2. AR Selection Constraints

a. National Weather Service

The first step was to identify AR events by day(s). Many studies of AR events look at integrated vertical transport (IVT) and total precipitable water (TPW), as these two together show the vertical forcing in combination with the tropical moisture needed for an AR. This study chose instead to look at surface precipitation observations over the 28-year period at the SF airport NWS station, as well as a NWS station to the north in San Rafael, CA, and to the south in Big Sur, CA, to corroborate the event using the data portal shown in Figure 12, where daily data for a month can be selected for a variety of locations, with precipitation totals provided for each location. A threshold of 1" of total daily precipitation at all three locations was used to determine a potential AR, as this quantity of precipitation per day across the broad swath of three weather stations along the CA coast is not usually seen in any other type of weather event (NOAA, 2022). Since the NWS is a U.S. government agency, they do not provide weather data for sites outside the U.S. The collection of Lisbon's precipitation data will be discussed in Section 4.

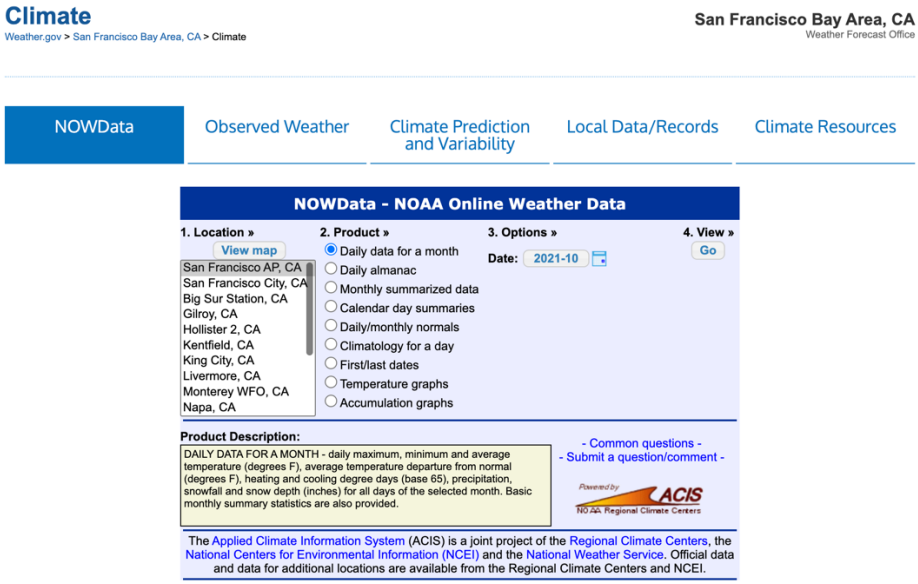

Figure 12. NWS daily weather archive data. Source: NOAA Climate (2022).

b. Precipitable Water Analysis

To ensure the high precipitation identified from the NWS analysis was in fact correlated to an AR event, the NOAA Physical Sciences Laboratory (PSL) portal was used to verify that a precipitable water "plume" was visible, indicating that the heavy rainfall was indeed tapping into a moist, ocean source, vice convection over land. IVT was not analyzed in the collection of these event dates, however the 1" threshold of daily precipitation combined with precipitable water plume was specifically chosen to weed out any convective or non-AR related precipitation events. Without the dynamical forcings associated with an AR, the CA Central Coast does not typically receive daily precipitation totals of greater than 1." This data analysis resulted in a total of 42 separate and distinct AR events during the 28-year period for the Central Coast of CA, with many of these events spanning multiple days. Figure 13 shows the long fetch precipitable water plume associated with the 24 October 2021 AR as it impacted the CA Central Coast.

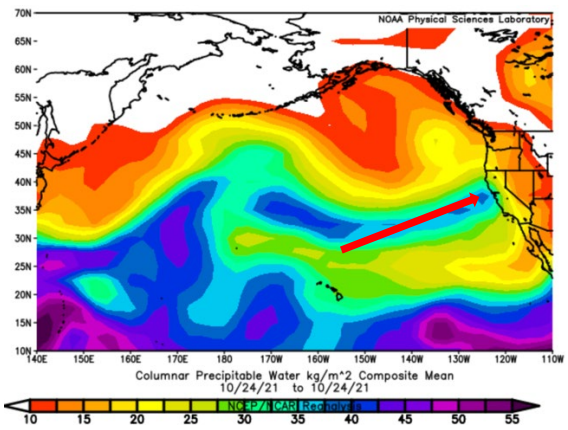

Figure 13. Total Precipitable Water average for 24 October 2021 AR event. Red arrow depicts the tropical source of precipitable water impacting CA. Source: NOAA/ESRL Physical Sciences Laboratory, Boulder Colorado from their website at http://psl.noaa.gov/.

3. Physical Sciences Laboratory Analysis

The NOAA PSL portal allows for the creation of monthly composites as well as daily composites of numerous variables from the climate forecast system reanalysis (CFSR) dataset. This was the initial resource used to identify the SFA value, as the

anomaly is more indicative of a persistent trend and departure from the mean (Kalnay, et.al, 1996). Plots allow for clear identification of areas of negative streamfunction anomaly shaded in dark purple, which is indicative of upper level troughing and upward vertical motion, and positive streamfunction shaded in orange and red, which is indicative of upper-level ridging and subsidence, and generally dry conditions. These visual streamfunction plots were used to identify the correlation and persistence of negative SFA as a predictor of ARs.

a. Composites of AR events

To identify a pattern in streamfunction for the AR events, the AR days for SF identified via 1" daily precipitation thresholds from the NWS site were input into the PSL site. A composite plot of 15 (16 entries is the max allowable on the PSL site) distinct AR events shows that a strong correlation is present between SFA and ARs at various timescales throughout the sub-seasonal timeframe (Figure 14).

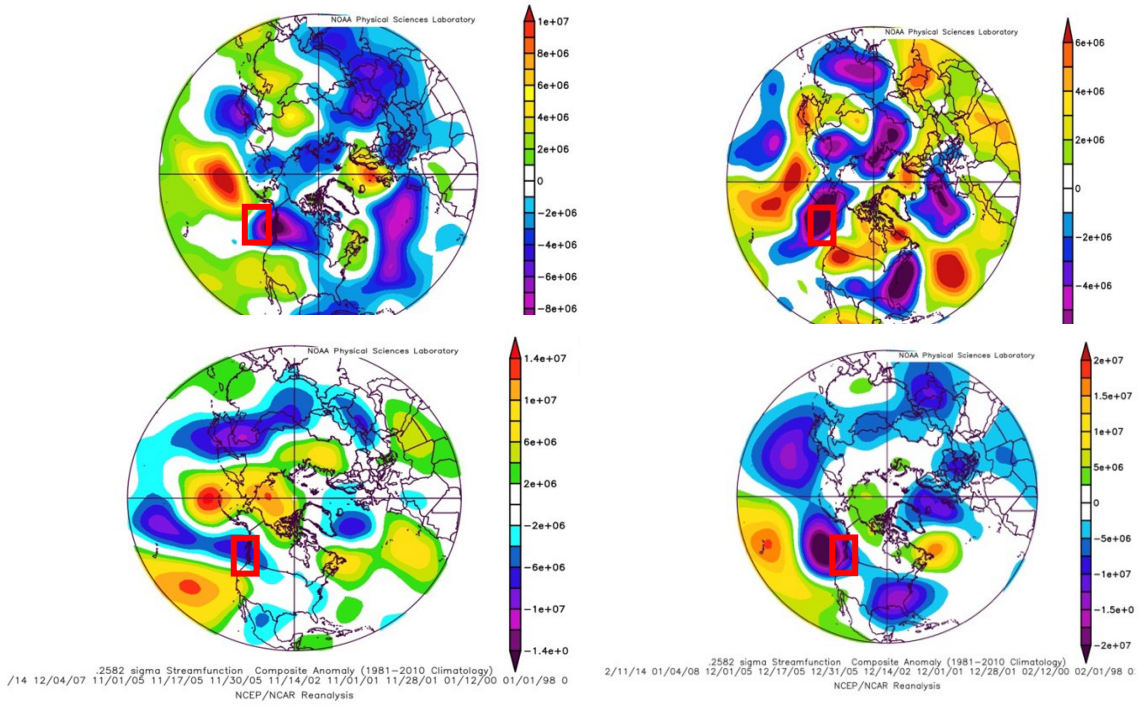

Figure 14. Northern Hemisphere view of the SFA plot at the .2582 sigma level (250mb), with analysis boxes overlaid in red. These plots show individual days centered on 15 separate AR events that impacted SF. Top left is 3 months prior to the AR events, top right is 2 months prior, bottom left is 1 month prior, and bottom right is during the AR events. This anomaly is calculated against the entire 1991–2020 climate reanalysis dataset. Source: NOAA/ESRL Physical Sciences Laboratory, Boulder Colorado from their website at http://psl.noaa.gov/.

Note the strong purple shading consistently present across the BC West Coast box identified in Figure 14. As previously outlined, this is negative SFA and is indicative of regions of upward vertical motion, which can be correlated with surface low pressure, synoptically supporting ARs for the CA Central Coast. What is most encouraging is that this signal is present at 90 days, far beyond the medium-range forecasting of 10–14 days. Not only that, but it persists at 60-days and 30-days prior to the event, suggesting a capacity for sub-seasonal forecasting.

b. Monthly event analysis

The previous analysis only captured SFA at single day snapshots, which can be misleading. Like geopotential height, it is very dynamic and transient on a daily interval. So SFA needed to be examined over longer intervals to confirm the signal wasn't shifting with each passing synoptic system. To do this, monthly composites were created for time periods prior to and around AR events.

To illustrate this monthly analysis, the AR event of 24 October 2021 was used. Multiple other events were analyzed by this process, but this specific event is highlighted based on its significance as an early season AR event for Central CA, dumping 4.02" of rain at the SF airport NWS station (NOAA, 2022). This monthly snapshot of SFA corroborates what was seen in the 15 event-composite from Figure 14. Figure 15 differs because it shows SFA across a consecutive 30-day period, with the image on the left capturing SFA 57 to 27 days prior to the AR event in question, and the image in the right capturing SFA 44 to 14 days prior to the AR.

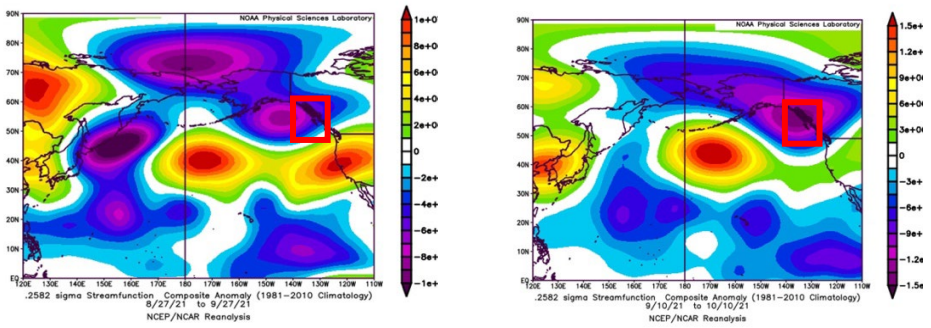

Figure 15. North Pacific view of SFA at .2582 sigma (250mb), with analysis boxes overlaid in red. These plots show 30-day periods prior to the 24 October AR event. The image on the left ends 27 days prior the AR event, and the image on the right ends 14 days prior. Source: NOAA/ESRL Physical Sciences Laboratory, Boulder Colorado from their website at http://psl.noaa.gov/.

In both timeframes a persistent, strong negative SFA is present in the BC West Coast focus region. This shows that the SFA signal may be persistent over relatively long periods, making it a viable sub-seasonal forecast variable.

c. 10-day event analysis

To examine the shorter period variability and refine the approach into something more valuable to a forecaster, composites were created with 10-day periods. Looking at this same event, 24 October 2021, of SFA in 10-day increments is shown in Figure 16. This would be more valuable to a forecaster utilizing SFA to predict the likelihood of AR events, by providing more frequent updates to the evolving pattern.

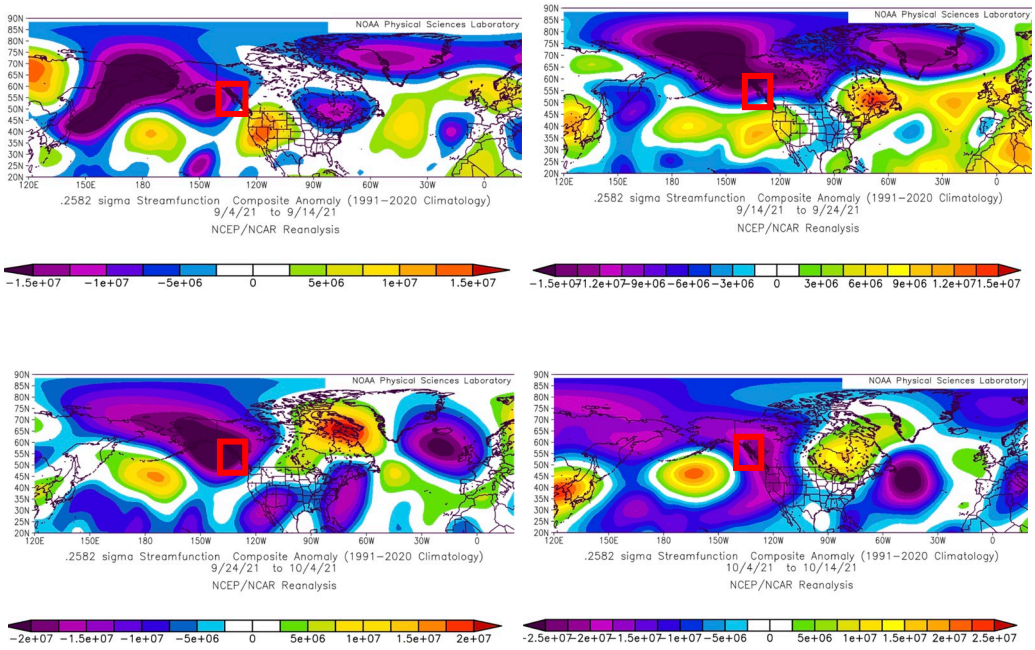

Figure 16. Northern Hemisphere view of SFA at .2582 sigma (250mb), with analysis boxes overlaid in red. These plots show 10-day periods prior to the 24 October 2021 AR event. Top left is 40–50 days prior, top right is 30–40 days prior, bottom left is 20–30 days prior, bottom right is 10–20 days prior. Source: NOAA/ESRL Physical Sciences Laboratory, Boulder Colorado from their website at http://psl.noaa.gov/.

Note that SFA is very strong in both the 10–20-day and 20–30-day windows in the BC West Coast focus region, with the signal becoming somewhat neutral beyond that.

Even if you were to narrow the PSL site product to the bounds of the latitude and longitude of the BC West Coast focus region, it would be hard to determine beyond the 30-day point if the SFA signal is predominantly negative or positive, or neutral. Additionally, the magnitude of SFA changes across timescales, making it subjective to conduct analysis solely on visual data. This level of ambiguity about the SFA value in a specific box led to the use of a numerical dataset, which is discussed in Section 4.

d. SFA lead

Now that the correlation between SFA was identified, the aim was to use this correlation in a way that would aid a forecaster in identifying the "signature" of the atmosphere at the sub-seasonal timescale, if possible. To create this metric, we used the PSL site to look within the BC West Coast box at the SFA variable. To capture SFA trends, each AR event date was used, and the SFA data analyzed. With the principal idea that a forecaster has a reliable model output of up to ten days (beyond which it becomes too chaotic to be reliable), the aim was to use SFA to give a forecaster an extended lead time- referred to as "SFA lead."

To quantify this, the average SFA value across the box was identified in 10-day windows working backwards from the AR event start date (not to include the actual event start date, as the signal is strongest). 10-day windows were chosen because the day-to-day variability of SFA, like any synoptic scale dynamic variable is high. Day to day analysis does not give an accurate picture of the larger temporal and spatial forcing being driven by SFA. Stepping backwards in 10-day windows, if the average SFA in the box region was negative, conducive to upward vertical motion as explained previously, then the SFA lead time was continued. When the average SFA during a 10-day window becomes positive during this backwards step process, then the SFA lead time was ended. For increased fidelity, the average was moved to find the specific day the negative SFA ended, still within a rolling 10-day window. For example, if the AR event occurred on 24 December, then the SFA average was analyzed from 14–23 December, 4–13 December, etc. Assuming the SFA average of the box turned positive from 4–13 December, then the 10-day window was shifted to 6–15 December and 7–14 December, until the specific day

was able to be captured. So, if it shifted on the 6th of December, that would result in a SFA lead time of 18 days. These were calculated across all AR events and plotted as a kernel density estimation (KDE), which are essentially heat maps, and will be discussed in the results section.

4. ERA5 Analysis

As previously mentioned, there was a level of ambiguity and subjectivity with the PSL site and utilizing SFA as it doesn't provide a total box average, but rather contour shading of values that vary throughout the box. To be able to tell numerically if the value was positive or negative, the Copernicus Climate Change Service (C3S) was utilized, as it provides a database with many variables. In particular, the Earth Reanalysis 5 (ERA5) is the European Centre for Medium-Range Weather Forecasts (ECMWF) climate reanalysis and has a dataset for both hourly and monthly averaged reanalysis data from 1959 to present, encompassing the timeframes needed for this study and provides specific numerical values across the box, which the PSL site could not offer. Since the ERA5 dataset does not have streamfunction as an available variable, a dynamically comparable one was used—the vertical integral of divergence of geopotential flux. This will be shortened and henceforth referred to as the divergence of geopotential flux (DGF). Negative SFA is synonymous with a positive value of DGF, and these variables are used interchangeably for the remainder of the discussion of this study. DGF is defined as the "horizontal rate of flow of geopotential, per meter across the flow, for a column of air extending from the surface of the Earth to the top of the atmosphere. Its horizontal divergence is the rate of geopotential spreading outward from a point, per square meter" (ERA5, 2022). DGF is a measure of energy propagation with large values being indicative of a large ageostrophic component of flow. A large DGF usually occurs in the mature stage of cyclone growth as energy is exported from the cyclone. Thus, large DGF would occur with a deep upper-level trough, which has a negative SFA.

To confirm that DGF and SFA are dynamically comparable variables that can be used for both analysis locations and for the numerical data analysis of this study, a comparison of the cumulative average across the 28-year period was done. Figure 17

shows the SFA plotted as a single value via monthly averages across the entire period of the study. Taking the same cumulative average of DGF resulted in the values seen in Table 1. At first glance, there appears to big difference between the DGF values of the two analysis boxes whereas for SFA they are quite similar. However, when the BC analysis box is adjusted with a statistical correction of -500 DGF, the two 28-year DGF values are nearly identical and match the magnitude and sign of SFA (slightly positive DGF=slightly negative SFA). The reason for this statistical correction will be discussed immediately following Figure 23.

Table 1. Cumulative average of 168 AR months utilizing DGF inside two analysis boxes.

BC West Coast box average (DGF)	Europe box average (DGF)
609.237	128.887

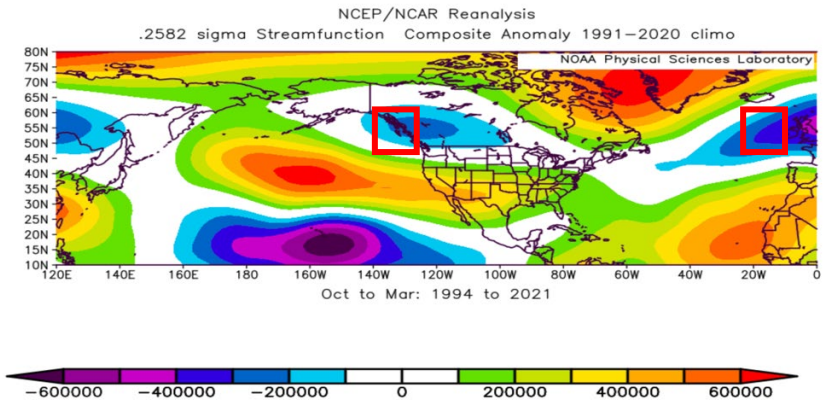

Figure 17. .2582 sigma (250mb) SFA average across all 168 AR months (ONDJFM) of the 28-year period (1994–2021) of this study, with analysis boxes overlaid in red. This anomaly is calculated against the entire 1991–2020 climate reanalysis dataset. Source: NOAA/ESRL Physical Sciences Laboratory, Boulder Colorado from their website at http://psl.noaa.gov/.

These similarities show that while SFA measures dynamical persistence and therefore perturbations, and DGF measures energy propagation, they are quantifying the same process of the atmosphere's conduciveness to cyclonic activity and therefore can be

used interchangeably in this study. DGF, as well as "total precipitation" from the same dataset, provided a comprehensive reanalysis dataset that were used to fully replicate what the NWS and PSL sites offered, with much more consistency both spatially and temporally.

Along with DGF, the ERA5 dataset variable 'total precipitation' was downloaded for the latitude/longitude of the SF Airport, 37.6°N, 122.4°W. This point was chosen to mirror the NWS location initially used to pull the precipitation data. As a finer temporal scale was needed for total precipitation, the dataset for precipitation was downloaded on the hourly scale, as no daily scale is available. Additionally, the precipitation data is in meters, so it was converted to inches (x 39.3701) and then summed over 24 times to give the desired result of inches of precipitation per day. The resulting data now represented reanalysis of the precise box region identified off the BC West Coast, as well as daily precipitation for the SF Airport, both for the 28-year period. As mentioned in the NWS section, Lisbon's precipitation data was not available from the NWS site, so the ERA5 dataset of total precipitation was also utilized for Lisbon, at 38.7°N, 9.1°W.

B. DATA VERIFICATION

Our dataset now consists of both visual (PSL) and numeric (ERA5) as well as observation (NWS) and model (ERA5) reanalysis data. Having identified the benefit of using the ERA5 reanalysis dataset and recognizing the limitations of standard observations when analyzing international locations, the next step was to conduct verification of the reanalysis data to ensure it was a viable substitute for Lisbon precipitation data. To show this, the ERA5 dataset was plotted against the NWS environmental observations over the timespan of 1994–2021 at the same location, the SF airport. Figure 18 shows this linear regression analysis, with a calculated regression coefficient of 0.966 and a standard error of the regression of 0.0145. This is an excellent result, as it shows the "goodness of fit" of almost 97%, confirming that the reanalysis data correlates with environmental observation data. The standard error is 0.01 inches, which is also well within acceptable error. This validates the use of the ERA5 dataset as a substitute for environmental observations.

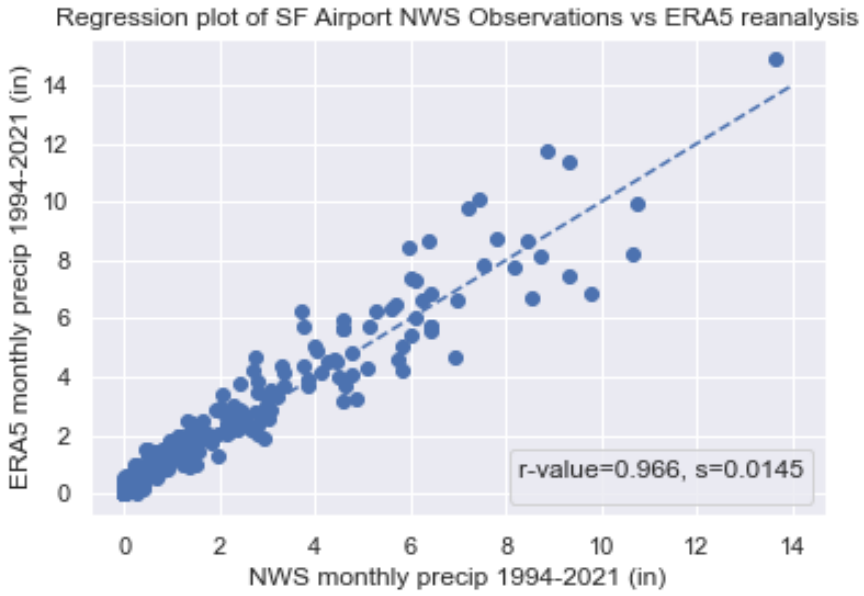

Figure 18. Linear regression analysis of monthly precipitation totals in inches of NWS observations and the ERA5 reanalysis dataset at SF airport between January 1994–December 2021.

C. MEASURING FORECAST QUALITY

An important aspect of any improvement to the forecasting process is the ability to quantify forecast skill, with the intent of identifying the operational application that this study's results could have. The methods in *Visualizing Multiple Measures of Forecast Quality* (Roebber, 2009) were used to accomplish this. A 2 x 2 contingency table was used to calculate our forecast skill. The variable that was being verified was streamfunction anomaly inside of the two box regions against an AR event. This was done for both locations, SF and Lisbon. The entire 28-year period, 1994–2021 was used, but only consisting of the climatological winter which is October-March, which is a total of 168 months. This allowed for a comprehensive analysis and skill score of the data used in this study. The lead times for predictors of AR events were:

1. SFA at 10–20 days prior to AR event
2. SFA at 20–30 days prior to AR event
3. SFA at 30–40 days prior to AR event

2x2 Contingency Table		Event Observed	
		Yes	No
Event Forecast	Yes	A	B
	No	C	D

Figure 19. Sample Contingency Table for establishing measures of forecast quality. A simple yes-no test is used to produce counts of the variables A, B, C, and D. Source: Roebber (2009).

Four variables are needed for the calculation of the contingency table. 'A' represents when the SFA forecasted an AR, that is, negative SFA, and in fact an AR event did occur--known as a "hit." 'B' was a forecasted AR event that did not occur, known as a "false alarm." 'C' was an event that SFA did not forecast, that is, positive SFA, but an AR event did occur; known as a "miss." Lastly, 'D' is a forecast of no event, and no event occurring, this is a "correct null." Using these variables, the calculation of metrics is possible.

The method of the contingency table allows for the mathematical calculation of accuracy, bias, reliability, and skill as illustrated in the equations below. Additionally, these results can be visually represented in a single diagram, which is referred to as a performance diagram and will be presented in the results sections of this thesis. Probability of Detection (POD) gives a measure between 0 and 1 of how successful the forecast is at predicting the event and is calculated:

$$\mathrm{POD} = \frac{A}{A + C},$$

False Alarm Ratio (FAR) gives an indication of when the forecast incorrectly predicts an event that the data verifies did not occur. The equivalent for FAR is Success Ratio (SR=(1-FAR)).

$$\text{FAR} = \frac{B}{A+B},$$

Critical Success Index (CSI) combines both POD and FAR to give the likelihood that the forecast will capture an event occurring, or its total success rate.

$$\text{CSI} = \frac{A}{A+B+C}.$$

Lastly, bias combines all the variables to determine if there is a trend favoring one aspect of the forecast versus another.

$$\text{bias} = \frac{A+B}{A+C}; \text{ or more simply, } \text{bias} = \frac{\text{POD}}{\text{SR}}$$

The desired result with these metrics for a good forecast is that POD, SR, CSI, and bias approach unity. The results of this analysis will be discussed in Chapter IV.

D. METHODS SUMMARY

Utilizing both observations and reanalysis data, a robust record of AR activity was created to verify SFA and DGF. The intent by using multiple metrics outlined in the methods section was to increase the granularity to specify what is AR driven, and "weed out" precipitation events that did not meet the criteria of an AR. By shifting our focus towards the ERA5 reanalysis data for the remainder of the study, the aim was to replicate what tools a forecaster would have for future AR events and their ability to extend the forecast of these events into the sub-seasonal timescale.

THIS PAGE INTENTIONALLY LEFT BLANK

IV. RESULTS

A. ANALYSIS OF NUMERICAL DATA

Visual analysis alone of SFA determined that there is a strong correlation between negative SFA and AR events and is an atmospheric tracer for AR events with sub-seasonal persistence. To quantify this relationship the ERA5 reanalysis data was used to analyze precipitation and the counterpart to SFA, DGF, on multiple timescales.

The first level of analysis was to take the known correlation of the negative SFA to AR events and apply it to the reanalysis dataset, which contains numeric values of equivalent DGF, removing the ambiguity of SFA that was discussed previously. Since individual AR events can occur relatively close together, this creates overlap in the periods preceding those events. If we focus on specific AR events, of which there were sometimes four in a month, there was no way to separate forcing prior to one event from the forcing during another event. To mitigate the problem of overlap from events, we quantified an "AR month" metric. This simplifies the data point to whether an AR event occurred during that month. If it did, it is an AR month; with no differentiation as to whether one or ten events occurred. If no AR event occurred during the entirety of that month, then it is not an AR month. This analysis of the 28-year period of 1994–2021 totals 168 months; hence 168 data points. Of those 168 months, SF had 42 months containing AR events and Lisbon had 32 months. Figure 20 shows the full year of data points on the left column of plots and the AR season (October-March) only on the right column of plots. Note that when excluding the April-September months, which is essentially climatological summer, no AR month data points are lost, and the signal excluded is primarily negative DGF, which is equivalent to positive SFA; which does not support AR activity.

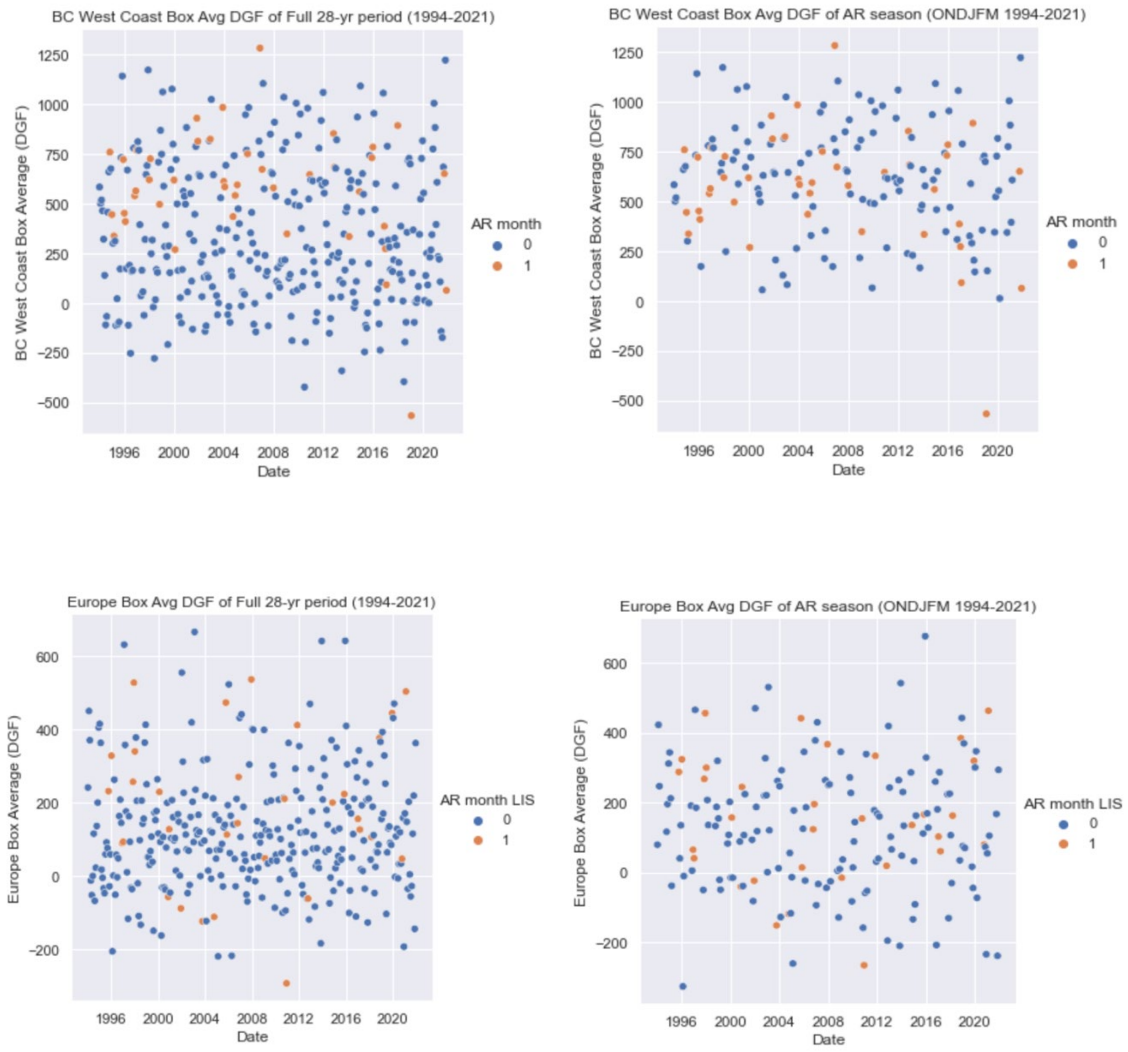

Figure 20. The plots show the DGF average over the focus regions of BC West Coast, top row, and GIUK, bottom row. The left column is all 336 months of the 28-year period while the right column is the 6-month AR season (168 months) only. Note the correlation between months where AR events occurred (shaded orange) and the DGF value.

The major takeaway from these plots is that what was observed in the visual analysis of the PSL SFA is confirmed by the DGF analysis. That is, AR events are strongly correlated with negative SFA (or positive DGF) for the month of occurrence in the two focus regions introduced in this study. There is a clear link between the DGF and the occurrence of ARs during an AR month. However, it is important to recognize that the range of DGF for AR months versus non-AR months is similar.

Since these plots do not show precipitation and one of the research questions asked if the intensity of the AR was dictated by the intensity of the SFA signal, the next step was to plot monthly precipitation totals vs. DGF to allow us to numerically answer this question. Figure 21 shows the total monthly precipitation for SF and Lisbon over the 28-year period. AR months are colored orange and generally have higher precipitation values. Almost exclusively, any month where large amount of precipitation occurred was tied to a month with an AR event, as seen by the heavy concentration of orange shaded data points at the top half of each plot. While it is generally expected that AR months have higher precipitation than non-AR months, the distributions do overlap. Statistical significance tests were not completed, but the mean precipitation for AR months is four inches or above while non-AR months is likely closer to one inch, which seem sufficiently distinct.

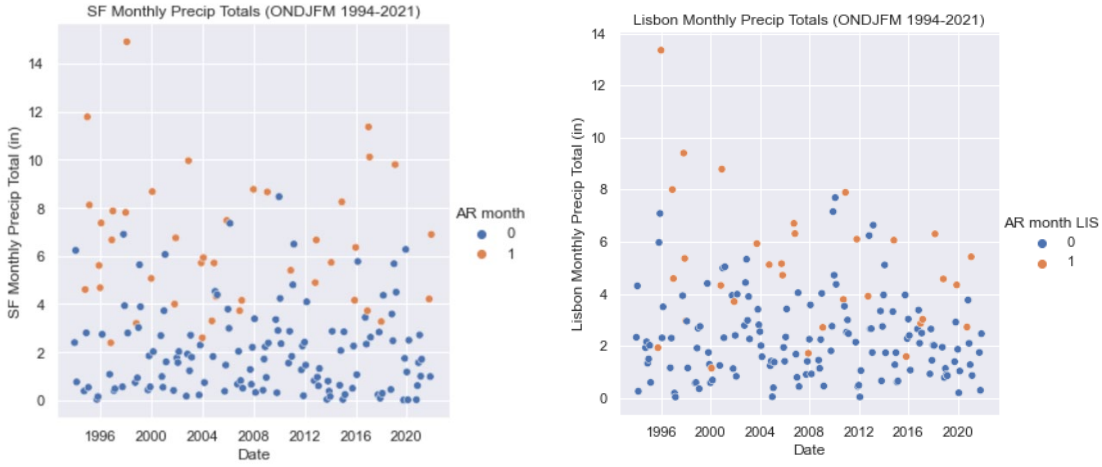

Figure 21. The plots show the monthly precipitation totals for SF, left, and Lisbon, right. This is plotted over the 6-month AR season only. Note the correlation between months where AR events occurred (shaded orange) and the high monthly precipitation.

Figure 22 shows the correlation between positive DGF and monthly precipitation. We see now that not only does a high positive value of DGF correlate with AR events, but it also appears for Lisbon that there is some correlation between the strength of the DGF and the strength of the AR, visually apparent as a transition of primarily blue dots in

the bottom left following a diagonal line to primarily orange dots in the upper right. This is corroborated by the data in Table 2. As noted previously, the spread in DGF for AR vs. non-AR months is very similar over all precipitation ranges. To quantify this, the average of AR month data points and non-AR months data points were calculated for both regions with the results shown in Table 2.

Table 2. Average DGF values for AR months and non-AR months of the BC West Coast box (left two columns) and the Europe box (right two columns).

	BC West Coast box average (DGF)	Europe box average (DGF)	
AR months (42)	573.388	157.544	AR months (32)
Non-AR months (126)	621.187	122.144	Non-AR months (136)

The results warrant further explanation, as the correlation of positive DGF with AR months only holds true for the Europe region, but not the BC West Coast region. This result is certainly not perfect, and it questions the viability using the argument of DGF as sub-seasonal forecast tool for ARs. However, a few reasons the correlation between positive DGF and ARs is still a viable one:

1. The European box average of DGF was greater for AR months than for non-AR months, so the use of DGF is validated in this region.

2. As identified in the prior research section in Chapter II, the BC West Coast box contains a climatologically more persistent region of negative geopotential height and therefore positive DGF. This is clearly seen by the significantly higher overall average of DGF compared to the European box and was the cause for the statistical shift discussed following Figure 23. These background climatological differences must be considered when comparing the results of the two boxes.

3. The prior research of Mundhenk identified the BC West Coast box as an area of significance for ARs impacting the entire West Coast of the U.S., not just the CA Central Coast. This thesis study constrained the results of an AR month to be one that impacted

SF exclusively, when a non-AR month very likely could have included an AR that impacted Washington, Oregon, or even Northern CA. Broadening the scope of AR landfall would possibly strengthen the correlation of positive DGF and AR months.

There is a correlation between the numerical analysis and the visual analysis discussed in Chapter III, and DGF is a valuable tool in analyzing ARs at the sub-seasonal timescale. It is important to note however, that further constraints should be made in addition to expanding the data collection to better understand the magnitude of the correlation between positive DGF and AR months.

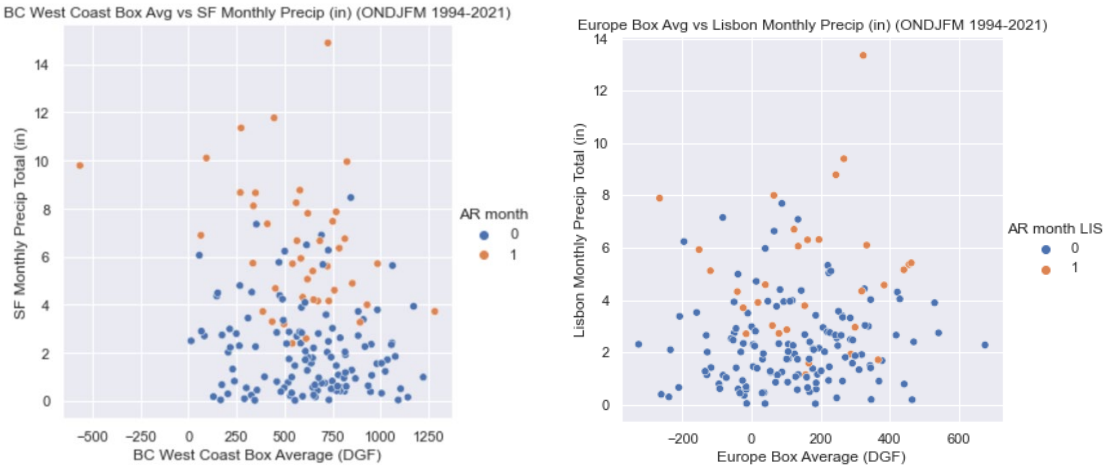

Figure 22. The plots show the DGF average over the focus regions of BC West Coast and GIUK vs. the monthly precipitation totals for each city respectively. Note the correlation between months where AR events occurred (shaded orange) and the DGF value and monthly precipitation.

Another way to interpret this data is in the form of a KDE, which uses a function that smooths out individual data points into a plot that appears visually like a heat map. Figures 23 plots the orange AR month data points only from Figure 22 for both analysis regions. This shows visually what the averages calculated for AR months in Table 2 are, with the added vertical axis of monthly precipitation to show the confluence of positive DGF and monthly precipitation for AR months.

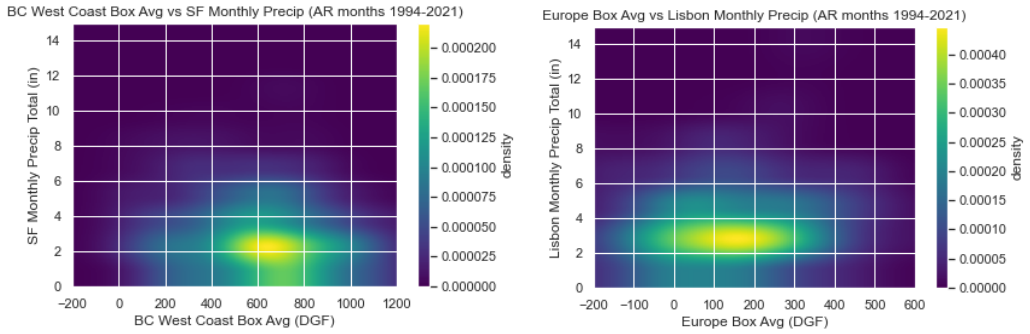

Figure 23. KDEs plotting AR months only of BC West Coast and GIUK DGF vs. the monthly precipitation totals. This is a smoothed function of the orange data points from Figure 22. Note the correlation between AR events and positive DGF for both locations.

A statistical trend that was identified from this analysis was that the DGF for the Europe focus region was centered on 0. Values greater than 0 correlated nicely with what was hypothesized about its relationship with AR events. Greater than 0 DGF (or negative SFA) should be indicative of upward vertical motion and therefore support AR activity and less than 0 DGF is the opposite. This correlates with how the data points fall as seen in Figures 20–22. However, for the BC West Coast focus region, that center point seems to be at around 500 DGF. Shifting our "center point" to 500 DGF for this focus region aligns our expected data with the results. This is represented by the red horizontal line on the plots in the next set of figures. The reason for this shift in DGF values between these two locations can also be understood as background climatological differences. While these two analysis regions are at the same latitudes in their respective ocean basins, the climatology of their upstream impacts likely varies significantly. The North Pacific appears to have a much more persistent trough based on the lack of negative DGF values. This could possibly be due to the length of the ocean basin upstream of the North Pacific box compared to the European box, but this theory and further analysis of the sensitivity of these regions was not analyzed in this study. Additionally, the topography of the coastline of British Columbia that is captured inside that box certainly enhances the DGF values, as vertical ascent forced by the topography of the Canadian Cascades creates large DGF values at the coastline. This is likely a significant contributor to the difference

in values between the two regions, as the Europe box is entirely over open ocean with no topographic impacts.

The overall relationship between DGF and SFA as well as AR occurrences and intensity have clearly been established in the preceding analyses. To be able to separate these relationships on smaller timescales and analyze yearly and monthly variation is also important. This was done by examining time series, which are shown in Figures 24 and 25. These line plots have the monthly DGF averaged across the focus region overlaid with the monthly precipitation total for the corresponding city. This allows for the temporal analysis of individual months in chronological order. Each panel captures seven years of data, and each data point represents a single month of the AR season (ONDJFM); except for the first data point of the top left panel in both figures, which begin with January of 1994. The line across each plot in Figure 24 (red) and Figure 25 (blue) indicate the threshold of DGF for each region over which an AR is expected, while the orange line across both figures indicates the threshold of 2" of monthly precipitation over which an AR is expected. Referring to Section 2 of Chapter III, the constraints for the identification of individual ARs was 1" of total daily precipitation. At the monthly timescale, a 2" total monthly precipitation was deemed the appropriate constraint to ensure only months with ARs were captured.

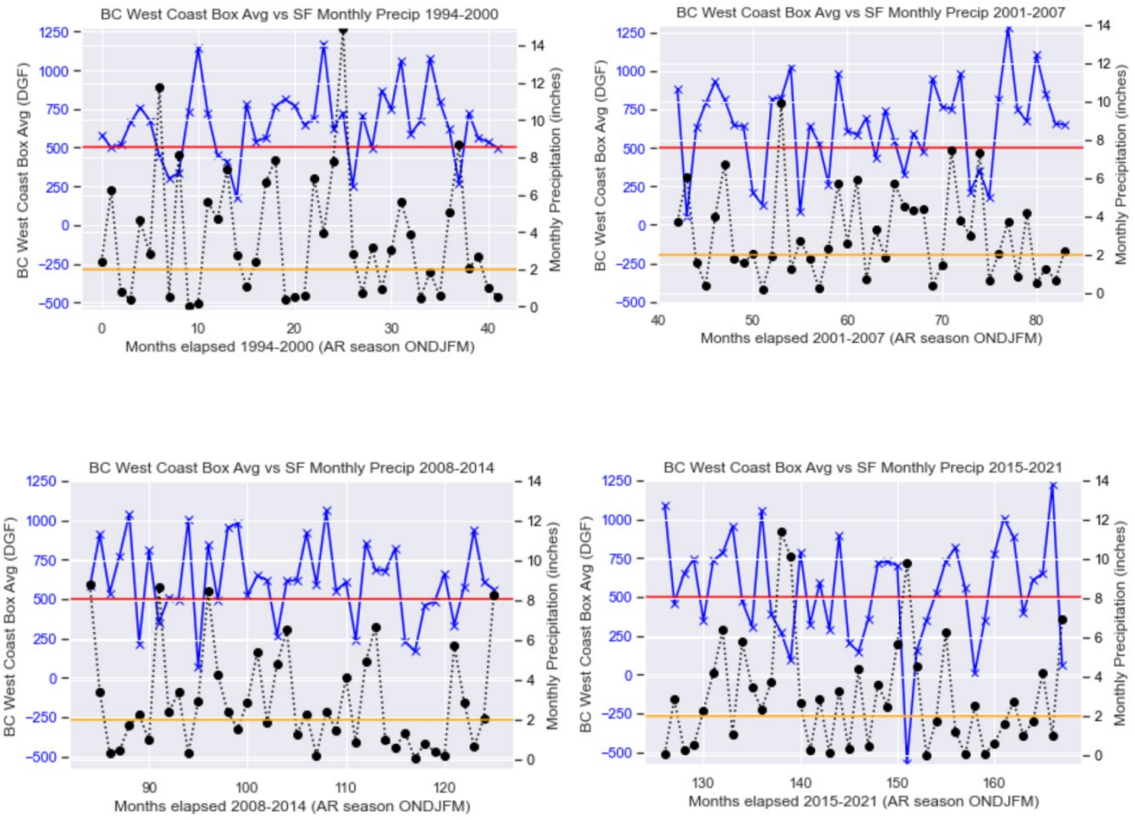

Figure 24. Time series plots of monthly DGF average of the BC West Coast box in blue versus monthly precipitation totals of SF in black. Time elapsed in number of months on x-axis, each plot is a seven-year increment. The red line indicates the threshold of 500 DGF and the orange line the threshold of 2" monthly precipitation over which an AR is expected.

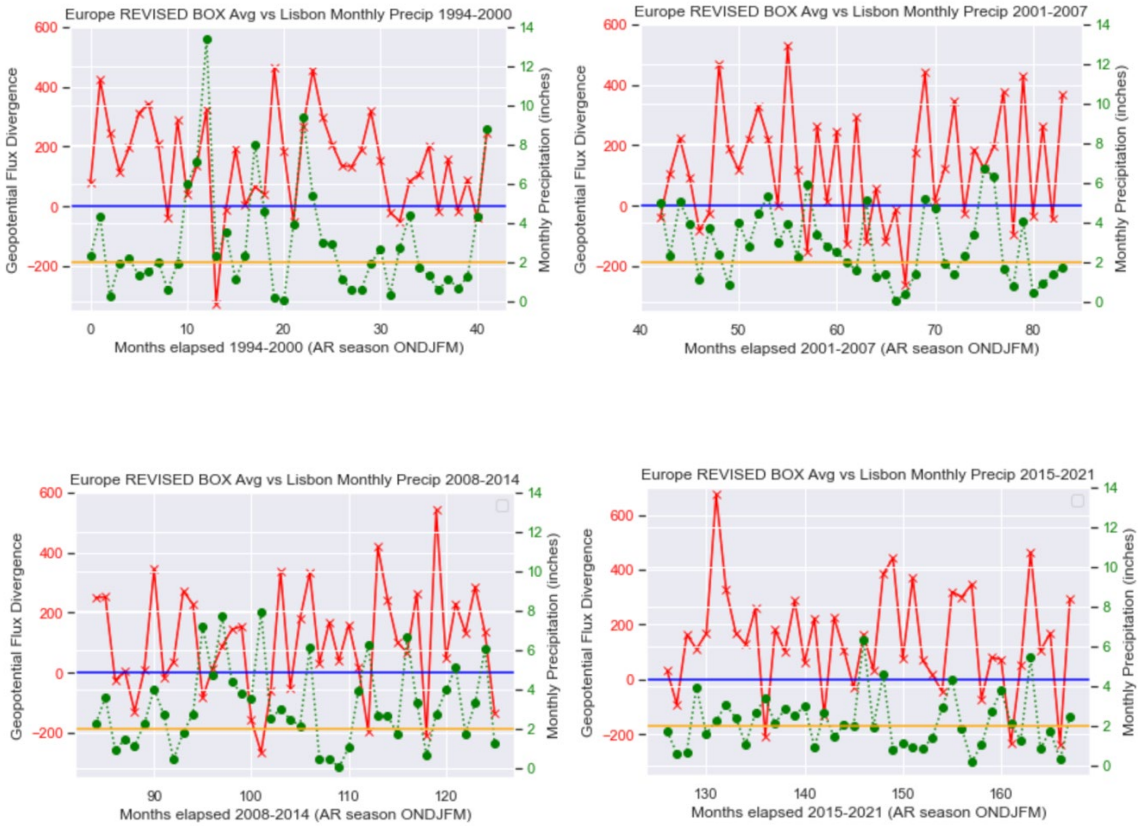

Figure 25. Time series plots of monthly DGF average of the Europe box in red versus monthly precipitation totals of Lisbon in green. Time elapsed in number of months on x-axis, each plot is a seven-year increment. The blue line indicates the threshold of 0 DGF and the orange line the threshold of 2" monthly precipitation over which an AR is expected.

In both Figures 24 and 25, we are looking for where the peaks match up. A spike in precipitation should be correlated with a spike in DGF, corroborating with what was observed in the scatter plot analysis. The time series analysis shows the monthly data point comparison of the two variables. While it is expected that high DGF should fit with high precipitation, it is understandable that not every single data point aligns with this expected outcome given the variability in DGF seen in the previous analyses. While there is good correlation between the two parameters for both locations, there are clearly periods where they vary in opposing directions. For example, the 1994–2000 period in Figure 25 (upper left) shows many periods where high DGF occurs with low precipitation. Other periods such as 2001–2007 (upper right) are much more strongly

correlated. To quantify this correlation, or lack thereof, each data point was binned into four categories shown below with the results displayed in Tables 3 and 4:

1. DGF & monthly precipitation > threshold
2. DGF > threshold > monthly precipitation
3. Monthly precipitation > threshold > DGF
4. DGF & monthly precipitation < threshold

Table 3. Bins of fit for data points from BC West Coast box DGF average vs. SF monthly precipitation total

BC West Coast box (DGF) vs. SF (monthly precipitation)	168 total data points	
	1. 61= 36%	2. 55= 33%
	3. 36= 21%	4. 16= 10%

Table 4. Bins of fit for data points from Europe box DGF average vs. Lisbon monthly precipitation total

Europe box (DGF) vs. Lisbon (monthly precipitation)	168 total data points	
	1. 76= 45%	2. 51= 30%
	3. 23= 14%	4.18= 11%

This process is similar to that of the contingency table, which was introduced in Section 3 of Chapter III, the difference being that this is using DGF vice SFA, it is the month average instead of the 10-day intervals preceding a specific AR event, and this is also incorporating a secondary constraint of monthly precipitation. The results that show correlation between DGF and monthly precipitation are 1) and 4), while 2) and 3) show that they are not correlated. As shown in Table 3, 46% of the data points for the BC West Coast box and SF are correlated, while 56% of the data points are correlated for the Europe Box and Lisbon.

Confining this result with one more added constraint, we now add the constraint on the positively correlated result (category 1) to be an AR month. Table 5 shows the results.

Table 5. Positively correlated data points from Table 3 and 4 with the added constraint of an AR month

Constraints	42 total AR months for SF, 32 total for Lisbon
BC West Coast box DGF >= 500, SF precipitation > 2," AR month	28= 67%
Europe box DGF >= 0, Lisbon precipitation > 2," AR month	22= 69%

The addition of the third constraint shows that DGF and monthly precipitation are indeed reliable indicators of AR activity. When an AR month occurs in these two regions, over two-thirds of the time DGF and monthly precipitation are positively correlated with the thresholds this study has set. This shows a good correlation between the two variables; however, it is worth noting that this is hindcasting which is strictly looking at past occurrences. Since the focus of this study was on forecasting at the sub-seasonal scale, Tables 6–11 in the next section focus on that aspect.

1. Individual Event Analysis

To show the relationship between DGF and SFA and precipitation, a few specific AR events have been highlighted and compared to the PSL output to demonstrate the initial visual analysis that was discussed in Chapter III. Figures 26–29 show instances of strong correlation between positive DGF and high monthly precipitation due to AR events across multiple different seasons and months. Each of these four figures shows the SFA anomaly alongside the DGF versus monthly precipitation for both regions. This process looked at the potential correlation of the two regions along the Rossby wave, with Figures 26 and 27 showing that correlation, and Figure 28 and 29 showing when they are not in phase. The analyses presented in these figures, where DGF and precipitation are overlaid alongside the SFA for the same period, corroborate the

dynamical connection of SFA and DGF, but more importantly their connection with spikes in monthly precipitation totals linked to ARs.

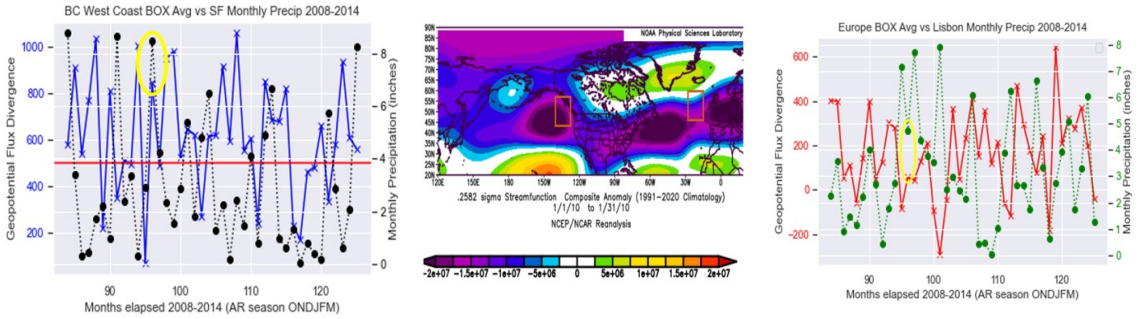

Figure 26. January 2010 AR events for both SF and Lisbon.

Note the strong correlation of peaks for both DGF and monthly precipitation in Figure 26.

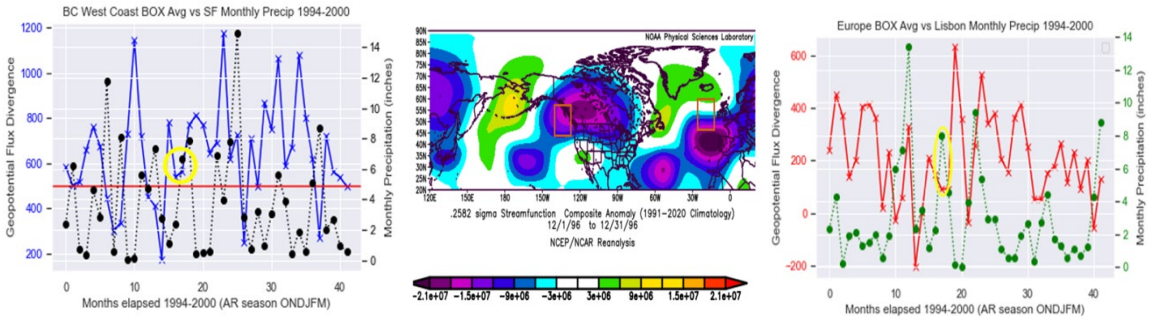

Figure 27. December 1996 AR events for both SF and Lisbon.

Note the strong correlation of peaks for both DGF and monthly precipitation in Figure 27.

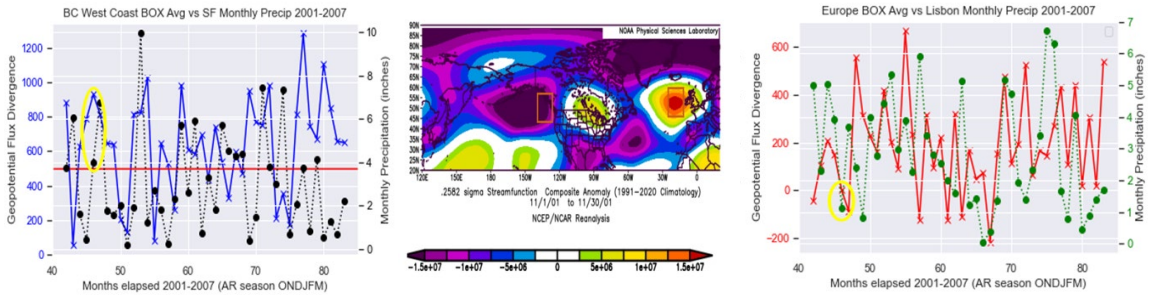

Figure 28. November 2001 AR event for SF only.

Note the inverse correlation of peaks for both DGF and monthly precipitation in Figure 28.

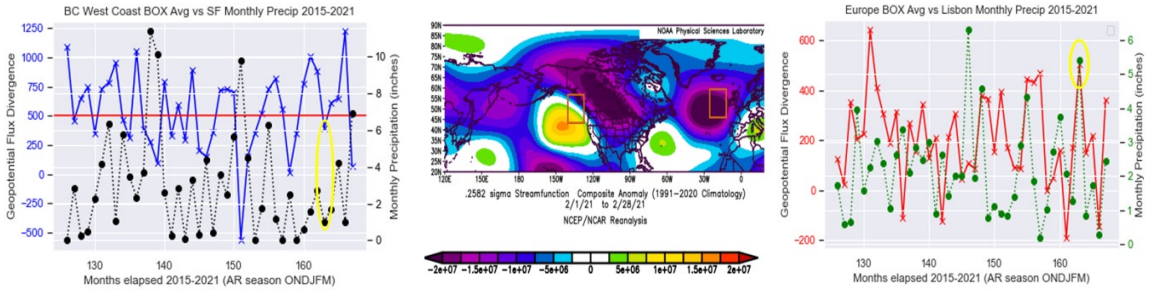

Figure 29. February 2021 AR event for Lisbon only.

Note the inverse correlation of peaks for both DGF and monthly precipitation in Figure 29. Figure 30 shows a potential area for future work that was identified during this study, where the inverse correlation between negative DGF and drought conditions may also exist and be useful for forecasting. Prior work by Kellen Jones titled "Wildfire-favorable offshore wind events in California: Global-scale Climate teleconnections to extreme weather and potential sub-seasonal to seasonal predictability" looked at this connection via SFA but did not utilize DGF.

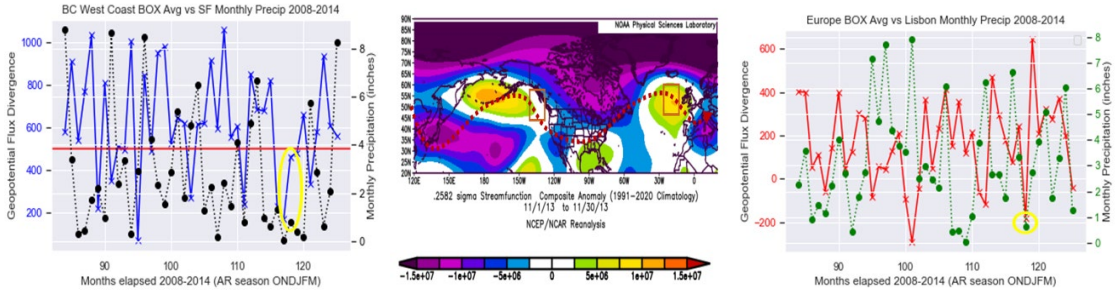

Figure 30. November 2013, no AR event for either city. Note the strong correlation of peaks in the negative direction for both DGF and monthly precipitation.

As the examples shown in Figures 26–30 illustrate, there are some periods where both regions have the same sign of SFA or DGF and others where they are of opposite sign. This suggests that the two regions can be linked but the relationship can be of opposite sign depending on Rossby wave setup. Further work is needed to better understand this relationship.

2. SFA Lead Results

Given the possible relationship found between DGA/SFA and AR occurrence and intensity for a given month, the question of how far in advance of an AR month could this signal be identified was investigated. Quantifying and categorizing the relationship into a way that could easily be used for forecasters was examined. This was introduced in section 3d. of Chapter III and referred to as "SFA lead." The idea is to quantify how long the SFA (with parallels to DGF) signal is present in a persistent state so the forecaster can use it as cueing to forecast AR events. By using the process previously discussed, the average SFA lead time of the BC West Coast box is 18.28 days and for the Europe box is 20.52 days. This means that prior to an AR event, the SFA signal was present and predominant in these two analysis regions for almost three weeks. These results are exciting because along with the previous results, it confirms that the correlation of SFA and precipitation for AR events exists beyond the current range of medium range forecasts and extends into the 2–5-week sub-seasonal forecasting window that this study aimed to reach. Additionally, the SFA lead time may be even greater because on several

instances, multiple AR events occurred back-to-back, within a few days of each other. The SFA lead was only extended during a period of no AR activity, so this may have lowered the lead time numbers a bit.

However, it should be noted that this calculation was done visually using the PSL plots and is at risk of significant subjectivity. Future studies may wish to replicate this process numerically to ensure a more robust analysis. Additionally, SFA lead was calculated off a known AR event, better known as "hindcasting." If this were to be applied more robustly to the entire 168-month analysis period with no knowledge of AR events, it may affect the SFA lead time.

B. ANALYSIS OF FORECAST SKILL

Figure 31 shows the result of the forecast verification introduced in section C of Chapter III. Common sense dictates that a good result is high correlation between forecasts and observations. The further the calculated variables fall along the dashed line to the upper right, the more accurate the forecast is. A good forecast occurs when POD, SR, and CSI approach unity; a perfect forecast would have all points lie in the upper right of the chart (Roebber, 2009). Additional observations of Figure 31:

(1) While the European points fall on the dashed line, the BC points are left of the line, with POD > SR, which corroborates with the preceding discussion in the results chapter. As discussed, the BC analysis box has a proclivity toward troughs in the analysis box, which corresponds to a high FAR and therefore a low SR.

(2) For both regions, the 10–20-day forecast is the most accurate, which is expected. However, the 20–30-day forecast is the least accurate, rather than 30–40-day. This may suggest that beyond 20 days, the "chaos" of the atmosphere becomes large, which is generally why models such as the GFS vary wildly beyond 10 days. A possible answer could be that in the 30–40-day cycle, they are in phase with Rossby waves. This also may show that streamfunction is a variable with dynamical persistence and has usefulness in analyses of sub-seasonal timescales. Further research would be needed to establish phase correlation regarding Rossby waves.

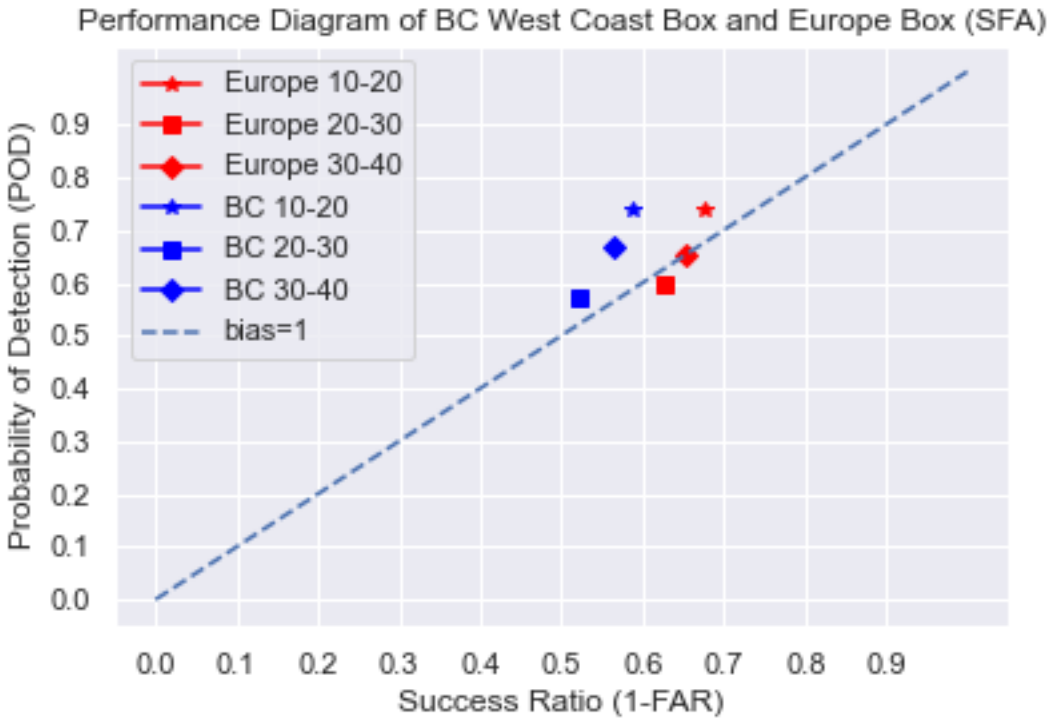

Figure 31. Performance Diagram of forecasted SFA at 10-day intervals vs. observed AR events. The red cluster of points are the European box forecasts, and the blue points are the BC West Coast box forecasts with a filter of DGF >=500.

Quantitatively, we can now populate the contingency tables with the analyses of three 10-day forecast periods, as introduced in section C of Chapter III. A focus on 10-day intervals was chosen as the most realistic and valuable for a forecaster to measure its usefulness. The process consisted of SFA analysis inside the bounds of each of the two boxes. The average SFA across the entire 10-day interval preceding an AR event was plotted and binned into one of the four contingency table variables (hit, miss, correct null, or false alarm). This was done for each of the three 10-day intervals, preceding each AR event in an AR month. If there were multiple AR events in a single AR month, the earliest event was used to not capture overlapping events. This was not always possible, so some overlapping of the forcing for multiple clustered AR events was impossible to avoid. The results of these calculations are shown in Tables 6–11. For quick reference,

exceedingly good results have been highlighted in green, and poor results highlighted in red.

Table 6. Europe box for the 10–20-day forecast.

Europe box (10-20-day forecast)		Event Observed (168 total months)		POD	0.737
				FAR	0.324
		Yes	No	SR	0.676
Event Forecasted	Yes	74	58	Bias	1.091
	No	26	9	CSI	0.545

Table 7. Europe box for the 20–30-day forecast

Europe box (20-30-day forecast)		Event Observed (168 total months)		POD	0.596
				FAR	0.372
		Yes	No	SR	0.628
Event Forecasted	Yes	60	58	Bias	0.949
	No	40	9	CSI	0.4403

Table 8. Europe box for the 30–40-day forecast

Europe box (30–40-day forecast)		Event Observed (168 total months)		POD	0.653
				FAR	0.347
		Yes	No	SR	0.653
Event Forecasted	Yes	67	58	Bias	1.0
	No	35	9	CSI	0.4853

Table 9. BC West Coast box for the 10–20-day forecast

BC West Coast box (10–20-day forecast) *Threshold of 500 DGF		Event Observed (168 total months)		POD	0.74
				FAR	0.413
		Yes	No	SR	0.587
Event Forecasted	Yes	31	88	Bias	1.26
	No	11	38	CSI	0.4868

Table 10. BC West Coast box for the 20–30-day forecast

BC West Coast box (20-30-day forecast) *Threshold of 500 DGF		Event Observed (168 total months)		POD	0.57
				FAR	0.477
		Yes	No	SR	0.523
Event Forecasted	Yes	24	88	Bias	1.089
	No	18	38	CSI	0.375

Table 11. BC West Coast box for the 30–40-day forecast

BC West Coast box (30-40-day forecast) *Threshold of 500 DGF		Event Observed (168 total months)		POD	0.67
				FAR	0.437
		Yes	No	SR	0.563
Event Forecasted	Yes	28	88	Bias	1.19
	No	14	38	CSI	0.4408

An analysis of the contingency tables shows both successful and interesting results. In both analysis regions, one would expect that as the forecast lead time increases, the SR, which is plotted along the x-axis of Figure 31, should decrease. This also means that the POD should decrease and FAR increase as the forecast lead time increases. For the most part, the results align with this expected outcome. Visually, this is reflected with the down and to the left trend of subsequent points as the forecast lead time increases.

Additionally, the scores for the European box were better, with a SR above 0.62 for all three periods, whereas the U.S. box had its SR drop down to 0.52. This trend has been a persistent theme across this study, with the Europe box forecasts better than the BC West Coast box, due to the persistence of the trough in the East Pacific during the winter months. While this study was initially focused on the impacts of ARs to the West Coast of the U.S., unexpectedly the shift in location to the Iberian Peninsula produced better forecast skill scores. It is therefore very promising that this technique can be applied to extend the forecast lead time of ARs potentially globally.

The scores for CSI further corroborate the promising results. A perfect score of CSI, nominally known as level of accuracy or total success rate, is 1.0, but the metric is not linear from 0 to 1 as with the other variables as the CSI values are contoured much

closer together from 0.4 to 1 than they are from 0 to 0.3 (Roebber, 2009). For this study, the CSI relative to climatology was 0.25 for the U.S. West Coast (42 AR months out of a possible 168= 0.25). With this climatology as a reference, a CSI greater than 0.25 is indicative of good accuracy and skill. Since the CSI scores from Tables 6–11 range from 0.37 up to 0.58, this is another validation of good forecast skill using SFA.

Lastly, the Heidke skill score (HSS) was calculated using the data from Tables 6–11 to provide an additional measure of forecast skill. HSS is valuable because it is measured against climatology, thereby measuring the forecast improvement over the standard (NOAA, 2003). It is calculated by taking the addition of "hits" and "correct nulls" from the contingency table, subtracted by the AR month total. This total is divided by the total number of months in the study, 168 in our case, subtracted by the AR month total again. HSS is measured on a -1 to 1 scale, with 0 being no better than a random chance, negative values worse than random chance (climatology in this case), and positive values showing forecast skill. Table 12 shows the calculated HSS, verifying the trend of better forecast skill for the European analysis region than the U.S. region, but most importantly for both regions, this study has produced valuable forecast skill for the sub-seasonal prediction of ARs.

Table 12. HSS of 10-day contingency table data shown in Tables 6–11

Europe box for the 10–20-day forecast	0.375
Europe box for the 20–30-day forecast	0.272
Europe box for the 30–40-day forecast	0.323
BC West Coast box for the 10–20-day forecast	0.214
BC West Coast box for the 20–30-day forecast	0.159
BC West Coast box for the 30–40-day forecast	0.190

THIS PAGE INTENTIONALLY LEFT BLANK

V. CONCLUSION AND FUTURE WORK

A. CONCLUSION

This research made significant efforts to draw a connection between using streamfunction and DGF as a tool to predict ARs at the sub-seasonal timescale. As shown throughout this paper, there is a strong correlation between streamfunction, its counterpart, the vertical integral of divergence of geopotential flux, and precipitation associated with ARs. This was demonstrated using a variety of methods and data sources, visually and quantitatively. ARs are an area of significant interest across a broad swatch of sectors and is ripe for continued research and improvements in forecasting. ARs have the potential to affect water usage of millions in the U.S. West alone and are sure to garner increased attention and funding in the years to come as water scarcity due to climate change continues to grow.

The analysis of forecast skill as quantified in Tables 6–11 shows that the method of using SFA and DGF as a tool for forecasters has a POD and SR of 60–70%, with the ability to aid in the sub-seasonal prediction of ARs with good success out to 40 days. This is a marked improvement from the current limitations of medium-range weather forecasts, which lose significant accuracy beyond 10 days. This validates the thesis goals of SFA being utilized as a predictive capability to help bridge the gap of forecasting in the sub-seasonal timescale.

Regarding our research questions introduced in Chapter II, we were successfully able to answer all three of them. This study showed that SFA and DGF can be used in place of geopotential height anomaly to provide forecasts at the sub-seasonal timescale with significant forecast skill, aiding a multitude of involved sectors with increased lead time in the prediction of ARs. The sub-seasonal forecast window remains ripe for growth, and this study has shown the benefits of research and analyses to bridge the gap between medium-range and seasonal forecasts. We successfully identified and refined the process for the anomaly box off the U.S. West Coast, which was first introduced by Mundhenk in his study. Most importantly, we were able to successfully replicate the anomaly box

process for the Southern Europe region with equally positive results. The groundwork has now been laid for continued replication to regions all over the world that are impacted by ARs. Lastly, there is a connection between strength of the SFA and the strength of the subsequent AR event(s), as quantified by total precipitation amount. However, due to the complexity of atmospheric and dynamical signals at play, this research question warrants further investigation to refine those results.

While there are many more complex atmospheric dynamics to consider regarding the forecasting of ARs, it is the hope and belief of this author that attention and awareness has been brought to the importance of this subject, and that these methods will be useful to aid forecasters in making more informed decisions and will increase the lead time for the involved communities.

B. FUTURE WORK

ARs occur throughout the world, so the concept of the streamfunction/vertical integral of geopotential flux divergence as an anomaly box to be used by a forecaster is a powerful concept. This study validated the anomaly box as a forecast tool providing lead time for AR events on the U.S. West Coast and the Iberian Peninsula of Western Europe. There is a clear path to replicate this process for major U.S. Navy operating areas off East Asia, specifically Japan, the Korean Peninsula, and the South China Sea, which would have tremendous implications for U.S. Navy operations. The climatology framework for ARs has already been created using the same dataset used for this study, ERA5 reanalysis (Pan and Lu 2020; Liang and Yong 2021).

The methods outlined in this study could be used to establish validated SFA regions, or "boxes" that provide forecasters sub-seasonal prediction of AR activity for regions throughout the world. This would aid emergency planners, water management agencies, and military planners who operate in the climatological regions of the mid-latitudes where ARs are so vital.

Much effort was made to correlate the two focus regions. There was hope that a clear correlation would occur with ARs on the CA Central Coast and the Iberian Peninsula, since they are climatologically similar and mirror each other in latitude. While

there was some correlation, not enough was shown to include it in this study, as further work into the dynamics of the Rossby waveguide relating to ARs needs to be done.

Lastly, there are a multitude of additional variables that could have contributing factors to forecasting at the sub-seasonal timescale that were not examined in this study. These include ENSO, Madden-Julian Oscillation (MJO), Quasi-Biennial Oscillation (QBO), and more. Analyses of these climate oscillations and phases in combination with the results found in this study could refine and narrow the scope of the results and provide further forecast skill and use.

THIS PAGE INTENTIONALLY LEFT BLANK

LIST OF REFERENCES

American Meteorological Society, 2022: Atmospheric river. Atmospheric river – Glossary of meteorology. https://glossary.ametsoc.org/wiki/Atmospheric_river (Accessed September 12, 2022).

Bbox Finder. *bbox finder*. http://bboxfinder.com/ (Accessed October 11, 2022).

Doiteau, B., M. Dournaux, N. Montoux, and J.-L. Baray, 2021: Atmospheric Rivers and Associated Precipitation over France and Western Europe: 1980–2020 Climatology and Case Study. *Atmosphere*, **12**, 1075, https://doi.org/10.3390/atmos12081075.

Dahl, J., 2022: Utilizing Earth Systems Prediction Capability (ESPC) to forecast Mistral wind events. M.S. thesis, Department of Meteorology, Naval Postgraduate School, 71 pp.

Google, 2022: Google Maps. *Google maps*. https://maps.google.com/ (Accessed September 12, 2022).

Guirguis, Kristen and Coauthors, 2018. Circulation drivers of atmospheric rivers at the North American West Coast. American Geophysical Union. 10.1029, 12,576-12,584.

Hersbach, H., Bell, B., Berrisford, P., Biavati, G., Horányi, A., Muñoz Sabater, J., Nicolas, J., Peubey, C., Radu, R., Rozum, I., Schepers, D., Simmons, A., Soci, C., Dee, D., Thépaut, J-N. (2018): ERA5 hourly data on single levels from 1959 to present. Copernicus Climate Change Service (C3S) Climate Data Store (CDS). (Accessed on < May-September 2022 >), 10.24381/cds.adbb2d47

Hersbach, H., Bell, B., Berrisford, P., Biavati, G., Horányi, A., Muñoz Sabater, J., Nicolas, J., Peubey, C., Radu, R., Rozum, I., Schepers, D., Simmons, A., Soci, C., Dee, D., Thépaut, J-N. (2019): ERA5 monthly averaged data on single levels from 1959 to present. Copernicus Climate Change Service (C3S) Climate Data Store (CDS). (Accessed on < May-September 2022 >), 10.24381/cds.f17050d7

Jones, K., 2021: Wildfire-favorable offshore wind events in California: Global-scale Climate teleconnections to extreme weather and potential sub-seasonal to seasonal predictability. PhD dissertation, Department of Meteorology, Naval Postgraduate School, 145 pp.

Kalnay, E. and Coauthors, 1996: The NCEP/NCAR Reanalysis 40-year Project. Bull. Amer. Meteor. Soc., 77, 437–471.

Liang, J., and Y. Yong, 2021: Climatology of atmospheric rivers in the Asian monsoon region. *Int J Climatol*, 41, https://doi.org/10.1002/joc.6729.

Mundhenk, B. D., Climatology and variability of Atmospheric Rivers over the North Pacific. PhD dissertation, Department of Atmospheric Science, Colorado State University, 98 pp.

Pan, M., and M. Lu, 2020: East Asia Atmospheric River catalog: Annual Cycle, Transition Mechanism, and Precipitation. *Geophys. Res. Lett.*, 47, https://doi.org/10.1029/2020GL089477.

PPIC, 2018: Shasta Lake California Drought. *Public Policy Institute of California*. https://www.ppic.org/blog/video-assessing-californias-global-warming-law/shasta-lake/ (Accessed March 1, 2022).

Ralph, F. M. and Coauthors, 2017. Atmospheric Rivers emerge as a global science and applications focus. Bull. Amer. Meteor. Soc., September 2017, 1969–1972.

Ralph, F. M., 2022: Better Atmospheric River forecasts are giving emergency planners more time to prepare for flooding. *Better Atmospheric River Forecasts Are Giving Emergency Planners More Time to Prepare for Flooding*. https://www.scientificamerican.com/article/better-atmospheric-river-forecasts-are-giving-emergency-planners-more-time-to-prepare-for-flooding/ (Accessed September 9, 2022).

Roebber, P. J., 2009: Visualizing Multiple Measures of Forecast Quality. *Weather and Forecasting*, **24**, 601–608, https://doi.org/10.1175/2008WAF2222159.1.

Smithsonian Magazine, 2021: Hoover dam's Lake Mead hits lowest water level since 1930s. *Smithsonian.com*. https://www.smithsonianmag.com/smart-news/hoover-dams-lake-mead-hits-lowest-water-level-1930s-180978022/ (Accessed October 10, 2022).

State of California, Department of Water Resources, 2022: California water watch. *Department of Water Resources*. https://cww.water.ca.gov/ (Accessed August 30, 2022).

U.S. Department of Commerce, N. O. A. A., 2022: NOAA Online Weather Data. *Climate*. https://www.weather.gov/wrh/climate?wfo=mtr (Accessed March 3, 2022).

U.S. Department of Commerce, N. O. A. A., 2003: Climate Prediction Center *Climate*. https://www.cpc.ncep.noaa.gov/products/predictions/short_range/verifications/html/srskill_exp.html#:~:text=CPC%20uses%20the%20Heidke%20skill,the%20%22worst%20possible%22%20forecast. (Accessed November 30, 2022).

Van Es, J., 2020: The interaction of Atmospheric Rivers and high-pressure systems. M.S. thesis Department of Meteorology, Naval Postgraduate School, 93 pp.

Zavadoff, B. L., and B. P. Kirtman, 2020: Dynamic and Thermodynamic Modulators of European Atmospheric Rivers. *Journal of Climate*, **33**, 4167–4185, https://doi.org/10.1175/JCLI-D-19-0601.1.

THIS PAGE INTENTIONALLY LEFT BLANK

INITIAL DISTRIBUTION LIST

1. Defense Technical Information Center
   Ft. Belvoir, Virginia

2. Dudley Knox Library
   Naval Postgraduate School
   Monterey, California